

Results of Airborne Field Measurements in the Antipodal Region of Radio Station NPM, Hawaii

J. E. ROGERSON

*Communication Branch
Radio Division*

April 26, 1966



U.S. NAVAL RESEARCH LABORATORY
Washington, D.C.

CONTENTS

Abstract.....	1
Problem Status	1
Authorization.....	1
INTRODUCTION.....	1
EXPERIMENT.....	2
INSTRUMENTATION.....	2
EXPERIMENTAL PROCEDURE.....	3
DATA REDUCTION.....	3
THE INDIVIDUAL ANTIPODAL FLIGHTS.....	5
First Antipodal Flight.....	5
First Flight Resumé.....	6
Second Antipodal Flight.....	6
Second Flight Resumé.....	7
Third Antipodal Flight.....	7
Third Flight Resumé.....	8
Fourth Antipodal Flight.....	9
Fourth Flight Resumé.....	10
Fifth Antipodal Flight.....	10
Fifth Flight Resumé.....	11
Sixth Antipodal Flight.....	11
Sixth Flight Resumé.....	12
Seventh Antipodal Flight.....	12
Seventh Flight Resumé.....	13
ANALYSES AND RESULTS.....	13
General Considerations.....	13
Field Strength Convergence.....	14
Diurnal Variations.....	14
Distance Dependency of Antipodal Fields.....	17
Phase Relationships of E and H	18
Comparison of Flights During Similar Ionospheric Conditions.....	19
Comparison of Similar Radials at Different Ionospheric Conditions.....	21
Departures from Simple Theory.....	21
CONCLUSIONS.....	23
ACKNOWLEDGMENTS.....	24
REFERENCES.....	24
FIGURES.....	25

Results of Airborne Field Measurements in the Antipodal Region of Radio Station NPM, Hawaii

J. E. ROGERSON

*Communication Branch
Radio Division*

The U.S. Naval Research Laboratory is conducting a comprehensive investigation of very-low-frequency (vlf) radio wave propagation. The objective of this investigation is to determine the parameters necessary for predicting the reliability of vlf communications in the ocean areas of the world.

It is believed that an investigation of the electromagnetic fields at and near the antipode of a vlf transmitter would provide much propagation information. Since all the antipodes of the Navy vlf transmitter stations, except for station NPM in Hawaii, are located in remote ocean areas, this makes them operationally difficult to investigate, especially with respect to navigation. The NPM antipode, however, is located on land near Ghanzi, Bechuanaland Protectorate, in the Kalahari Desert in southern Africa. Navigation in the vicinity of the NPM antipode could conceivably be more precise than in other antipodal areas.

An analysis of the data obtained in July 1963 by the Naval Research Laboratory via aircraft flights in the vicinity of the antipode of radio station NPM, Hawaii (19.8-kHz transmitter) is presented. Definite evidence of convergence of field strengths was found, as expected; a peak value of 2.0 mv/m for the field was measured during the experiment. Indications of an inverse square root dependence on distance for the field strength were observed. The expected diurnal pattern of highest field strengths at local sunrise, lowest fields at local sunset, and intermediate fields at local noon and midnight was found to be true. However, the antipodal situation appeared to be complex; suggestions of movement of the electromagnetic antipode were seen. Navigational difficulties contributed to uncertainties in the data and made definite conclusions difficult to obtain. The Navy Electronics Laboratory, San Diego, California, participated in this experiment by recording amplitude data at fixed ground sites around the geographic antipode and also phase data aboard the same aircraft. When the data taken by the two laboratories are combined, more comprehensive results may be obtainable.

INTRODUCTION

In July 1963, the U.S. Naval Research Laboratory (NRL) and the U.S. Navy Electronics Laboratory (NEL) conducted a joint radio wave propagation experiment in the vicinity of the antipode of the U.S. Navy very-low-frequency (vlf) transmitting station NPM at Lualualei, Hawaii. This report deals with the analysis of that portion of the data gathered by NRL aboard a Navy WV-2 aircraft in flight in the immediate vicinity of this antipode, which is located in the southern portion of Africa.

If the earth and the ionosphere are treated as a spherical waveguide, as is done in vlf radio wave propagation theory, there is an area on the side of the earth opposite the transmitter in which the signals arriving over the multitude of propagation paths converge; this area of convergence

is called the antipodal region. In the idealized case in which the earth and the ionosphere form a homogeneous, isotropic, spherical waveguide and the transmitter is a vertical dipole, this convergence occurs at a single point which is geometrically opposite the transmitter. The electric field strength E is at a maximum at this point, and the magnetic field strength H has a minimum value at this point because of the phase relationships of the various converging signals. In this case the geographic antipode and the electromagnetic antipode are spatially coincident. In the region immediately around the antipode, the field strength E varies as the absolute magnitude of the zero-order Bessel function, and the envelope of the field strength curve varies as the inverse square root of the distance from the antipode. The converging signals form a standing wave pattern in which the nulls of either E or H are separated spatially by half a wavelength. Antipodal effects have been treated theoretically by Wait (1), Crombie (2), and Norton (3).

NRL Problem R01-39; Project SR 008-01-01, Task 7044. This is the final report on one phase of the problem; work is continuing on other phases. Manuscript submitted Nov. 3, 1965.

Experimental evidence of antipodal focusing has been found by Round, *et al.* (4) and Crombie (2). In February 1962, a joint experiment was conducted by NRL (5,6), NEL, and DECO Electronics, Inc., Boulder Laboratories, in the vicinity of the antipode of the Navy transmitting station NAA at Cutler, Maine. A peak NAA antipodal field strength of 3.7 mv/m was recorded. This is approximately the field strength that would be measured at a distance of 4000 km from NAA over an all-seawater path under daylight conditions. Since the antipode is approximately 20,000 km from the transmitter, the recorded peak field of 3.7 mv/m represents a definite convergence effect. Asymmetric field patterns around the antipode were detected, but this result was expected since the earth-ionosphere waveguide is neither homogeneous nor isotropic.

Most of the antipodes of the Navy vlf transmitters are located in remote ocean areas; for example, the antipode of NAA is located in the Indian Ocean about 800 mi from Perth, Australia. Consequently, serious operational and navigational difficulties are encountered. A measurement of antipodal field patterns requires many measurements over a large area; hence, an airplane is more useful than a ship. However, an aircraft requires a base of operations, and since such airports are usually so far removed from the antipode, the amount of time available for aircraft maneuvers in the antipodal vicinity is very limited. The remoteness of the antipode from land areas means that there are no navigation beacons or recognizable landmarks in the antipodal vicinity.

The transmitting station NPM, in Lualualei, Hawaii, has its antipode on land. This antipode is located near Ghanzi, Bechuanaland Protectorate, in the Kalahari Desert in southern Africa. In planning the experiment, it was believed that this inland site would provide the following advantages:

1. the possibility of finding an aircraft base of operations much closer to the antipode than otherwise possible;
2. the possibility of installing ground recording sites in the antipodal vicinity to continuously monitor signals in that area; and
3. the possibility of finding recognizable landmarks that could be used as navigational aids.

(When this is the case, the difficulties due to the lack of navigational beacons in the area can be partially overcome.)

In theory, then, the NPM antipode offered an opportunity for a more thorough and precise study than is possible at the antipodes of the other Navy vlf transmitting stations.

EXPERIMENT

Several overall aims were established in planning the experiment. The primary purpose of the experiment was to measure the amplitude and phase of the antipodal fields and to determine the field patterns in the vicinity of the antipode. A determination of the position of the electromagnetic antipode relative to the geographic antipode was desired. The experiment was also designed to measure the diurnal variations in the position, amplitude, and patterns of the electromagnetic antipode. A further aim of the experiment was a study of the attenuation rates for the various propagation paths converging at the antipode.

The experiment was divided into two operations—continuous monitoring of the NPM signals by fixed-station receiving sites on the ground in the antipodal vicinity, and measurements conducted at various times of the day aboard an aircraft flying prescribed patterns through the antipodal area. The ground-based sites, operated by NEL, continuously recorded the amplitude of the NPM signals; these sites contained loop-antenna instrumentation for determining the directions of arrival of the received signals. Aboard the aircraft, phase data from a vertical omnidirectional whip antenna were recorded by NEL, and amplitude data from a vertical monopole antenna and two vertical crossed loops were recorded by NRL. Data from cardioid-pattern antennas were taken by NRL also. This report concerns only the data recorded by NRL; in-flight phase data and ground-station amplitude data are to be analyzed by NEL.

INSTRUMENTATION

Suitable vlf field strength and phase recording equipment were installed aboard one of the NRL "flying laboratories," a Navy WV-2 aircraft. A

vertical, 2-m whip antenna and two vertical crossed loops located in the upper radome permitted omnidirectional reception of vertical E and horizontal H fields. The multicoupler used with the antennas allowed simultaneous operation of several vlf receivers and provided a variable-bearing cardioid pattern. The effective heights (*i.e.*, calibration factors) of the antennas were determined experimentally to permit absolute field strength measurements. The phase of the received vertical electric field was recorded relative to a rubidium frequency standard.

As a navigational aid, a doppler radar navigation system was installed in the aircraft. This system was designed to provide very accurate ground speed and drift angle information about the aircraft motion; the output of this system was recorded on Esterline Angus charts. The navigator's instrument panel was photographed automatically at 3-min intervals and by manual command whenever the aircraft changed heading. Thus a continuous record of the aircraft motion was to be provided. As another navigational aid, a transponder beacon was placed on the ground near the geographic antipode. This beacon was tuned to the frequency of the aircraft's regular radar, and it transmitted back to the aircraft the pulse received from the aircraft radar. The purposes of the transponder beacon were to pinpoint the destination area more precisely and to increase the range of the radar system. As will be pointed out later, neither the doppler radar system nor the transponder beacon functioned well, and both were of little use in carrying out the experiment.

EXPERIMENTAL PROCEDURE

As the base of operations for the WV-2 aircraft, the Jan Smuts Airport near Johannesburg, South Africa, was chosen. The distance from this point to the antipode is approximately 450 naut mi; this distance is well within the capabilities of the WV-2 aircraft, and thus several hours were available for maneuvering in the antipodal vicinity.

The original planning of the experiment called for eight local flights in the area around the geographic antipode. For each of the local ionospheric conditions—sunrise, noon, sunset, and midnight—two flights were planned. Each flight

consisted of three radials through the antipodal region. Each radial was designed to pass through the geographic antipode and to extend outward about 90 km on either side of this focal point; the ends of the radials were to be joined by arcs centered at the geographic antipode. For each local ionospheric condition, alternate flight patterns which traversed each radial in opposite directions were to be used for the two flights. In planning the experiment, it was believed that day-to-day repetition of the antipodal field patterns and possible movements of the electromagnetic antipode would be more detectable by using repeated radials than by using a different set of radials for each flight.

The radials were selected in such a way as to take advantage of the particular situation. One radial was chosen to lie along what was expected to be the direction of arrival of a strong signal; the others were chosen to make use of the few radio beacons in the area.

Due to unforeseen difficulties, the actual experiment differed somewhat from the planned experiment outlined in the preceding paragraphs. Only seven local antipodal flights were possible; the noon flight was not repeated. The failure of the doppler radar system and the transponder beacon to function properly contributed greatly to navigational problems. The transponder beacon did not operate for some reason as yet unknown, and it was later established that the doppler radar system had a variable error which made its output unreliable and unusable. Thus, navigation was much less accurate than the original project goals. These uncertainties led to deviations from the desired flight plans and resulted in greater difficulty in the analysis of the data. No attempts were made to fly arcs centered at the geographic antipode because of navigational difficulties.

The actual flight patterns did essentially traverse each radial in opposite directions on the pair of flights for a given local ionospheric condition. A list of correspondences among the various flights is given in Table 1.

DATA REDUCTION

The uncertainty in the knowledge of the aircraft's position made reconstruction of the actual flight patterns from the navigator's logbooks more difficult. By accepting certain points, such

TABLE I
Correspondence of Flights in the Vicinity
of the NPM Antipode

Local Sunset		
<u>First Flight</u>		<u>Fifth Flight</u>
First radial	{ Corresponds to }	Second radial
Second radial		Third radial
Third radial		First radial
Local Midnight		
<u>Second Flight</u>		<u>Sixth Flight</u>
First radial	{ Corresponds to }	Third radial
Second radial		First radial
Third radial		Second radial
Local Sunrise		
<u>Third Flight</u>		<u>Seventh Flight</u>
First radial	{ Corresponds to }	Third radial
Second radial		First radial
Third radial		Second radial

Note: The fourth flight was a local noon flight and was not repeated due to operational difficulties.

as celestial fixes and visual observation of known landmarks, as being correct, other points in the flight pattern were determined by "dead reckoning." In other words, from the aircraft bearing and ground speed at a given time, its position at a future time was estimated.

The coordinates of these known points, the time at which the aircraft was located at each point, the assumed ground speed between each pair of points, and the coordinates of the geographic antipode were fed into a digital computer, which then calculated the bearing and the distance of the aircraft from the geographic antipode as functions of time. These results were then plotted as polar plots of the flights, with the geographic antipode as origin.

By using the output of the computer program and the listings of the field strengths as functions of time, it was possible to construct plots of the field strengths *vs* distance from the geographic antipode. In the planned flight patterns in which all the radials went through the geographic antipode, all field strength points along a given radial would be at the same bearing from the geographic antipode. In the actual flights,

very few of the radials passed through the geographic antipode; therefore, in the field strength *vs* distance plot for a given radial, the bearing relative to the geographic antipode was constantly changing. (Of course, in the planned flights, the bearing relative to the geographic antipode would change by 180 degrees as the aircraft passed through this point.)

A large part of the analysis was based on these plots of field strength *vs* distance from the geographic antipode. Thus, the problems in navigation resulted in a lack of precise position information, which in turn contributed to uncertainties and difficulties in analysis. Often, necessities for the aircraft to change course in the antipodal vicinity added further complication to the analysis and interpretation of the data.

Another concept used in the analysis is that of resolving the received field strengths into a major and a minor component. This is based on the assumption that the field strength at any point in the vicinity of the antipode can be resolved into two components, and that it is the amplitude and phase relationships of these two components along the path of flight of the airplane that produce the oscillatory variations in the field strength. The respective amplitudes of the two components were deduced from the data by assuming that the average voltage of adjacent maxima and minima was the amplitude of the major component, and the deviation of the maxima and minima from the average was the amplitude of the minor component. The time assigned to the major and the minor component values is the average of the times of the consecutive maximum and minimum field strengths. Plots of the major components of the field strength *vs* distance from the geographic antipode were made and used in the analysis and are given at the end of this report.

A monitor receiver was operated in Washington, D.C., during the experiment, and the data taken in the antipodal vicinity was compared with data recorded by the monitor to identify locked-key transmissions and off periods.

All of the data plots are presented at the end of this report. On some of the field strength *vs* distance plots, time advances to the right, while on others, time advances to the left. As pointed out earlier, the flight patterns were so designed that on repeated flights the radials were traversed

in opposite directions. Plotting the data in this way made comparisons of similar radials easier because the data observed on a given side of the geographic antipode during the flights appeared on the same side of the origin in these plots.

THE INDIVIDUAL ANTIPODAL FLIGHTS

In this section of the report, some comments are made on the individual antipodal flights. The flights are analyzed, radial by radial, and the implications of the data for each flight are summarized. Reference is often made in this section to Figs. 1(a)-(d) which present the pre-experiment calculations of the antipodal field strengths and azimuthal behavior; these plots are explained more fully in the Analyses and Results section of this report. The polar plots of the individual flights, with the geographic antipode as origin, are given in Figs. 2(a)-(g). Figure 3 is a plot of the function $f(d) = -10 \log |d|$, which was used to investigate plots of the field strength major components *vs* the distance from the geographic antipode. Figures 4 through 10 are plots of the measured field strengths and the calculated field strength major components for each radial.

The electromagnetic antipode was assumed to be the largest value of electric field intensity measurable in the antipodal vicinity. The position of the electromagnetic antipode was not expected to be coincident with the geographic antipode and could have varied with time.

In this section of the report, the geographic antipode is called the GA and the electromagnetic antipode is referred to as the EA. All field strengths (except in Fig. 1) are given in decibels (db) relative to 1 microvolt per meter. All bearings from the geographic antipode, as well as all aircraft headings, are given in degrees relative to true north (TN). All times are given as Universal Time (UT).

First Antipodal Flight

The first local antipodal flight was made on July 14, 1963, under conditions of local sunset at the antipode. The calculated field strength polar plot for local sunset is given in Fig. 1(a), and the polar plot of the first flight radials is given in Fig. 2(a). The aircraft remained in the antipodal vicinity from about 1430 UT to about

1840 UT. Since ionospheric sunset occurred at about 1642 UT at the antipode, the aircraft was in the antipodal region for a period extending from about two hours before local sunset to about two hours after local sunset.

First Radial—The maximum *E* field strength of 49 db recorded on the first radial did not occur until the aircraft had passed the GA and was at a distance *d* of approximately 14 kilometers (km) and a bearing of 187°T from this point. The signals appeared to be building up according to a $d^{-1/2}$ law until the aircraft reached a point about 36 km (210°T bearing) from the GA; at about this point, the aircraft heading changed from 224° to 231°T. After this change in direction, the field strength dropped sharply, and the $d^{-1/2}$ behavior was lost. This drop was not explainable by looking at the calculated field strength polar plot of Fig. 1(a), and would probably not be expected to be as large as the measured decrease. However, the plot in Fig. 1(a) did indicate that this pass should be along the direction of arrival of a strong signal; thus some $d^{-1/2}$ behavior might have been expected and was observed. The relative amplitudes of the *E* and *H* fields were apparently 180° out of phase in the approach to the GA. The total measured field strength plot for this pass is shown in Fig. 4(a); the calculated major component plot is shown in Fig. 4(b).

Second Radial—The measured field strength *vs* distance plot for the second radial is shown in Fig. 4(c), and the calculated major component *vs* distance plot for this radial is shown in Fig. 4(d). This pass missed the GA by about 26 km, as compared to a miss distance of only about 8 km for the first pass. The maximum field strength of 51.5 db occurred about 30 km from the GA at a 225°T bearing; this peak value was 2.5 db higher than the peak value on the first pass. On this second pass, a field strength level of 43.5 db was recorded about 27 km from the GA at a bearing of roughly 255°T, followed by another peak of 50.5 db at a distance of 30 km and a bearing of 282°T. The minimum value would thus seem to be about midway between the two maxima and at a distance of about 14 km from each. If, as was expected, adjacent maxima and minima would be separated by a quarter of a wavelength along the direction of a strong signal, then the angle between the aircraft heading and the strong-signal direction would be about 74°. Since the

aircraft heading was 344°T , the strong-signal direction could be 270° , 058° , 090° , or 238°T . The field strength polar plot of Fig. 1(a) predicted strong signals arriving from approximate bearings of 280° , 95° , 150° , and 210°T . The flight track was not expected to be along a strong-signal bearing, and no strong-signal effects, such as $d^{-1/2}$ behavior, were observed. After the second maximum, the signal level decreased gradually. The sudden increase in signal level at a point approximately 36 km and a bearing of 211°T from the GA could not be accounted for, except perhaps as a sunset, day-night discontinuity line effect.

Third Radial—The measured field strength *vs* distance plot for the third radial is shown in Fig. 4(e), and the calculated major component *vs* distance plot for this radial is shown in Fig. 4(f). The radial passed by the GA at a distance of about 8 km and in a direction of 105°T . The maximum field strength recorded on this pass was 53 db; this maximum occurred about 42 km from GA at a bearing of about 275°T . On the approach to the GA, $d^{-1/2}$ behavior was quite evident, as expected, and the *E* and *H* fields were approximately 180° out of phase in the occurrence of their maxima and minima. After the occurrence of the peak field strength, the signal level decreased slowly; it did not appear that the $d^{-1/2}$ relation was obeyed very closely in the region east of the GA. The polar plot of Fig. 1(a) indicated that a strong directional effect, such as $d^{-1/2}$ dependence in field strength, might be expected on this pass, and this phenomenon was observed.

First Flight Resumé

The peak values of field strength on this flight were always observed in areas west of the GA; it might thus appear that the EA was west of the GA. Because of the higher peak observed on the third radial, it would seem that this pass came closer to the EA than the other passes; it is possible that the peak on the third pass represented the EA field strength at that time. It is also very probable, because of the duration of the flight and the sunset transition period at the GA, that the EA moved during the flight. From the first to the third passes, the positions of the peak field strengths occurred successively further west of the GA; this tendency might indicate that the EA moved westward during the flight, or that the

EA was stationary and that the three passes successively passed closer to its position, or both of these situations.

Second Antipodal Flight

The second antipodal flight was made on July 15-16, 1963, under midnight conditions at the GA. The polar plot of the calculated field strengths at local midnight is given in Fig. 1(b), and the polar plot of the flight radials is given in Fig. 2(b). The aircraft was in the antipodal area from about 1930 UT to about 2330 UT.

First Radial—The plot of the measured field strength *vs* distance and the calculated major component *vs* distance for the first pass are given, respectively, in Figs. 5(a) and (b). As the GA was approached, the field strength appeared to be building up according to the $d^{-1/2}$ relation. Interference effects were observed, with the relative phase relationships of the *E* and *H* maxima varying between 0° and 180° . The $d^{-1/2}$ behavior was observable on the departure from the GA but was not as definite as on the approach. A maximum *E* value of 55 db was observed at approximately 24 km and a bearing of 309°T from the GA. A similar peak in *H* occurred nearby such that the separation of the *E* and *H* peaks was about 4 km, or $\lambda/4$. The polar plot of Fig. 1(b) indicated that this pass should have been along the direction of arrival of a strong signal; a strong-signal direction behavior, such as $d^{-1/2}$ dependence of the fields, was observed. As may be seen from the polar plot of Fig. 2(b), the aircraft heading on this pass was about 283°T , and the flight missed the GA by about 11 km.

Second Radial—The measured field strength *vs* distance and the calculated major component *vs* distance for the second radial are shown in Figs. 5(c) and (d). This radial was complicated by aircraft maneuvers. The aircraft approached the GA at a heading of 52°T until it reached a point at about 77 km and a bearing of 219°T from the GA; at this point, the aircraft assumed a heading of 35°T and continued past the GA. Along this segment of the flight path, the aircraft passed by the GA at a distance of about 6 km and a bearing of about 300°T . At a point 15 km and a bearing of 13°T from the GA, the aircraft assumed a 47°T heading, which was maintained until the aircraft moved out of the immediate

antipodal vicinity. The average signal level remained fairly steady throughout this radial. (This behavior could be best seen in the calculated major component plot.) Interference phenomena were not very noticeable, and $d^{-1/2}$ behavior was not very evident. The field strength polar plot in Fig. 1(b) suggested that this pass should have been along the direction of arrival of a strong signal, but no strong-signal direction effects were noted. If a strong signal arriving from a bearing of 280° to 300°T predominated, the aircraft would have been flying in a direction that was roughly normal to the direction of arrival of this strong signal, and a relatively constant signal level would be expected. The polar plot of Fig. 1(b) suggested a strong signal from a 280°T direction.

Third Radial—The plots for the measured field strength and calculated major component *vs* distance from the GA are given in Figs. 5(e) and (f), respectively, for the third radial of this flight. A peak *E* field strength of 57.5 db occurred at about 50 km and a bearing of 302°T from the GA. The field strengths built up faster than $d^{-1/2}$ on approaching the peak and decreased faster than the $d^{-1/2}$ relation on leaving the peak. The polar plot in Fig. 1(b) suggested that this radial would be along a weak-signal direction, and the absence of a $d^{-1/2}$ dependence appeared to indicate agreement. There was some evidence of interference phenomena. This radial was also complicated by aircraft maneuvers, as can be seen from Fig. 2(b). The aircraft entered the antipodal area at a heading of 160°T but changed to a heading of 135°T at a distance of about 96 km from the GA. This heading was maintained until a point at a distance of 11 km and a bearing of 220°T from the GA was reached; at this point a heading of 140°T was assumed until the aircraft had reached a point at 54 km and a bearing of 152°T from the GA. Then a heading of 170°T was assumed until the aircraft left the antipodal vicinity.

Second Flight Resumé

The *E* field peaks on the first and third radials were nearly equal; the difference in levels was 2.5 db. They might have represented the EA field at the times of their measurements, or they might have represented similar peaks in the EA field pattern at these times. The peaks were

spatially separated by 27 km and time separated by about 3 hr; the information suggested that perhaps the EA moved approximately 27 km in a 295°T direction in the 3-hr time interval between measurements. Another possibility was that the two peaks represented different maxima in a stationary antipodal standing wave pattern; if this were so, both passes should have recorded other peaks that would be similarly separated. Such peaks were not observed, however.

Third Antipodal Flight

The third antipodal flight was made on July 17, 1963, under local sunrise conditions. The aircraft was in the vicinity of the GA from about 0035 UT to 0435 UT. Since ionospheric sunrise occurred around 0434 UT, the aircraft was leaving the GA vicinity at about the time sunrise was occurring. This flight was then terminated in Capetown instead of returning to Johannesburg. The polar plot of the calculated antipodal field strength patterns at sunrise is given in Fig. 1(c), and the polar plot of the flight radials is given in Fig. 2(c).

First Radial—As seen in the data plots in Figs. 6(a) and (b) for the first radial, the field strengths built up to a value that remained fairly level as the aircraft passed near the GA at a distance of about 6 km and a bearing of 200°T . This "plateau" was attained about 60 km east by southeast of the GA; the field strength level centered around 50 db. The aircraft was flying in a 289°T direction until it reached a point that was 10 km distant from the GA at a bearing of about 245°T ; then a heading of 300°T was assumed. Peaks of 60 db for *E* and *H* were then recorded. The *E* peak occurred at approximately 52 km from the GA and a bearing of 291°T ; the *H* peak occurred at about 56 km from the GA at roughly the same bearing. The *E* and *H* peaks occurred approximately one quarter of a wavelength apart. No good evidence of $d^{-1/2}$ behavior was observed on this radial. After the observed peaks, the field strengths decreased more rapidly than a $d^{-1/2}$ dependence. The polar plot of Fig. 1(c) suggested that this radial should have displayed strong-signal direction effects. If the predominant signal were coming from a bearing of 210°T , the fairly steady field strength level near the GA could be explained as being due to motion of the

aircraft normal to this strong signal direction. The peaks could be the result of constructive interference between this signal and a weaker signal from a bearing of 280° or 290° T. The field strength then might decrease quite rapidly as the aircraft left the antipodal vicinity, as was observed.

Second Radial—The second pass missed the GA by about 26 km at a bearing of 125° T. The aircraft approached the antipodal region from the southwest at a heading of 65° T until it reached a point 84 km at a bearing of 201° T from the GA; the aircraft then assumed a 39° T heading and maintained this direction throughout the rest of this radial. The measured field strength and calculated major component *vs* distance plots are shown in Figs. 6(c) and (d). No well-defined peaks were observed; the signal level increased rather slowly and steadily from roughly 40 db to about 55 db throughout this pass. There was some evidence of an interference pattern in the region southwest of the GA. About 120 km northeast of the GA, the signal attained this 55-db level, which was maintained for a large distance; there was little evidence of an interference pattern on this part of the flight. The polar plot in Fig. 1(c) suggested that this pass should have shown the effects of motion along the direction of arrival of a strong signal, but no $d^{-1/2}$ dependence in the field strength was observed. There was little evidence of interference phenomena. A single dominant signal at the antipode from the northwest (approximately 310° T bearing) or the southeast (approximately 130° T bearing) could have produced the field strength behavior observed on this radial. However, this strong-signal direction contradicts the strong-signal direction postulated to explain the data behavior on the first radial. In order to agree with this postulate, the second radial would have to show strong directional effects, which were not observed.

Third Radial—The measured field strength and calculated major component plots for the third radial are shown in Figs. 6(e) and (f). This radial passed the GA at a distance of 3 km and a bearing of about 250° T; the heading of the aircraft was 151° T, and this direction was maintained throughout this pass. The field strength curve apparently reached a minimum about 150 km northwest of the GA; then the field strength built up to a peak value at a distance of 44 km and a bearing of 328° T from the GA. The minimum *E* value was

about 37.5 db, and the peak value was about 61 db. After this peak, the field strength stayed fairly level, maintaining an average value around 57 db until after the aircraft had passed the GA. After the aircraft reached a point at about 60 km and a bearing of 153° T from the GA, the field strength decreased. Very little evidence of interference phenomena was observed on this pass; the calculated major component plot did not show any $d^{-1/2}$ behavior anywhere; the *E* and *H* fields appeared to vary in the same manner as though only a signal from a single propagation path were present. The polar plot of Fig. 1(c) suggested that this pass should be along a weak-signal direction; the behavior of the field strength data in the immediate vicinity of the GA suggested that this portion of the radial might be normal to the direction of arrival of a strong signal, and the decrease in signal level before and after the aircraft passed the GA also agreed with this idea. If this radial were normal to a strong-signal direction, then it would be expected from the plot of Fig. 1(c) that the strong signal would be coming from a direction of about 240° T. It should be noted that this pass was made just as sunrise was occurring at the GA, and the nearness of the day-night transition could have produced additional effects.

Third Flight Resume'

Evidence of an interference pattern was seen on the entire first radial but was only slightly indicated on the other two passes. The positions of the peaks on the first and third passes suggested that the EA might be somewhere northwest of the GA; since these peaks were approximately of the same amplitude, they might have represented two crossings of the same equal-amplitude contour around the EA. Since the field strengths on the second pass were lower than these peak values, it would then appear that the EA was northwest of the GA. If, on the other hand, these peaks represented the EA field strength at the times of their observation, then the first and third pass results suggested that the EA had moved approximately 30 km in a 55° T direction in a period of about 3 hr. The relatively steady field strengths observed in the second pass might have indicated a strong direction of arrival from a 310° T or a 130° T direction. The results of the first and third passes suggested the 310° T direction. Therefore,

if the first and third radials did not pass through the EA, perhaps it could be assumed that the EA was in the sector between the passes, with an angular width of approximately 30° .

Fourth Antipodal Flight

The fourth flight to the NPM antipodal vicinity was performed on July 25, 1963, under conditions of local noon at the GA. The polar plot of the calculated antipodal field strength patterns at noon is given in Fig. 1(d). A polar plot of the flight radials is given in Fig. 2(d). The aircraft was in the immediate vicinity of the GA from about 0615 UT to about 1030 UT.

First Radial—The first radial approached the GA at a heading of about 285°T and passed this reference point at a distance of 11 km and a bearing of 195°T . At a point 50 km from the GA and a bearing of 272°T , the aircraft assumed a new heading of 296°T . The measured field strength and calculated major component *vs* distance plots are given in Figs. 7(a) and (b), respectively. From a distance of about 180 km east of the GA, the signal level increased in a $d^{-1/2}$ manner to an *E* field peak of 61.5 db at a point about 30 km from the GA and a bearing of 263°T . The *E* and *H* maxima occurred simultaneously. There was little evidence of interference phenomena on the approach to the peak values, but after the peak occurred and the aircraft assumed its new heading of 296°T , interference effects became more evident. The field strength decreased quite rapidly after the peak value occurred, but after the new heading was taken, a smaller peak ($E = 50$ db) occurred at a distance of 86 km and a bearing of about 280°T from the GA, after which the field strength decreased more slowly. A $d^{-1/2}$ dependence in the field strength was seen in the approach to the GA but was not seen after the occurrence of the peak field strength. It also appeared that the *E* and *H* fields maintained a constant phase relative to each other throughout this radial.

Second Radial—The measured field strength and calculated major component *vs* distance plots for the second radial are shown in Figs. 7(c) and (d), respectively. From a point approximately 120 km from the GA, the field strength rose gradually as the aircraft approached the GA at a 57°T heading. At a point 36 km from the GA and a bearing of

211°T , the aircraft changed to a 41°T heading, and the signal dropped sharply. However, at a point about 18 km from the GA and a 202°T bearing, the aircraft heading changed to 45°T , and the signal strength returned to the level observed just before the aircraft changed from its 57°T heading; this level was approximately 53 db. The aircraft then passed the GA at a distance of 7 km and a bearing of 140°T . Another dip in signal level ($E = 46$ db) occurred about 26 km from the GA at a bearing of 61°T . Another peak ($E \approx 56$ db) occurred at approximately 50 km and a bearing of 54°T from the GA. After this peak, the signal level decreased gradually as the aircraft left the immediate vicinity of the GA. There was some evidence of interference effects on the approach to the GA but no evidence of such effects during the departure from this point. According to the polar plot in Fig. 1(d), this radial should have been along a strong-signal direction of arrival, but no $d^{-1/2}$ dependence was definitely observed. The dips in the signal level occurring in the proximity of the GA cannot be explained by looking at Fig. 1(d); these minima are probably the results of interference of signals arriving from two or more directions. These minima were separated in distance by about 46 km; the last two peaks were separated by about 50 km. Allowing for the uncertainty in the aircraft position and speed, these two distances could easily be identical. Assuming a half wavelength separation between maxima (or minima) along a strong-signal direction, this result would suggest that the aircraft was flying at an angle of approximately 80° to a strong-signal direction. A strong signal direction would then be a bearing of 125° , 145° , 305° , or 325°T . The polar plot of Fig. 1(d) suggested that the 305°T direction would be the most probable choice.

Third Radial—Figures 7(e) and (f), respectively, show the measured field strength and the calculated major component *vs* distance from the GA for the third radial. This radial maintained a heading of 160°T throughout the vicinity of the GA and passed this point at a distance of 4 km and a bearing of 70°T . There was good evidence of interference phenomena on this entire pass, but especially in the approach to the GA. The variation of the *E* and *H* fields appeared to be approximately 180° out of phase, with the separation of the maxima and minima of both fields being of

the order of 4 to 8 km. A peak E field value of 55 db occurred at a distance of 18 km and a bearing of 354°T from the GA; the H field peak occurred nearby at a distance of 20 km from the GA at roughly the same bearing. A secondary peak occurred approximately 48 km from the GA at a bearing of 155°T . Both on the approach to the first peak and on the departure from the second peak, the data on this pass roughly obeyed the $d^{-1/2}$ dependence, although the origins for the $d^{-1/2}$ plots were not coincident. The calculated field strength plot of Fig. 1(d) indicated that this pass should be along a weak-signal direction, but phenomena associated with a strong-field direction were observed.

Fourth Flight Resumé

The position of the EA was difficult to determine from the data on this flight. Since the highest peak occurred west of the GA on the first radial, it might seem that the EA was westward of the GA; however, signal levels only a few db lower were recorded north and northeast of the GA on the other radials. These results could have indicated that the EA was somewhere close to the GA and that the aircraft was passing near the EA but not through it.

Fifth Antipodal Flight

The fifth flight was the second local sunset flight and was performed on July 26, 1963. The radials are plotted in Fig. 2(e); the applicable field strength polar plot calculations are shown in Fig. 1(a). The aircraft was in the vicinity of the GA from about 1204 UT to about 1600 UT. Since ionospheric sunset occurred roughly at about 1642 UT, the aircraft left the area before ionospheric sunset. However, ground sunset occurred at about 1605 UT, just as the aircraft was ending the last pass.

First Radial—The first radial maintained a 290° heading throughout the vicinity of the GA, which was missed by 2 km at a bearing of 200°T . The measured field strength and calculated major component *vs* distance plots for this radial are shown in Figs. 8(a) and (b). On the approach to the GA, the signal strength increased gradually to a peak value of about 50 db, which occurred at a point about 8 km from the GA and a bearing

of 125°T . After the aircraft passed by the GA, the signal level dropped sharply, as can be seen best in the calculated major component plot in Fig. 8(b). Interference phenomena were apparent throughout this radial, but especially after the GA was passed. Maxima and minima differences of the order of 10 db were observed and, in the region to the west of the GA, it was noted that the calculated major components of E and H varied in different manners, *i.e.*, they did not follow similar patterns. Some evidence of a $d^{-1/2}$ behavior was observed in the area far to the east of the GA on the approach; the data in the range from 170 km to about 90 km showed this behavior. Such behavior was not observed elsewhere on this pass. The polar plot of calculated field strengths in Fig. 1(a) suggested that the direction of this radial should be close to two, approximately opposite, strong-field directions. However, at this time of day, many strong-signal directions were predicted so that a complex field strength pattern might be observed for this whole flight.

Second Radial—The pertinent data plots for the second radial are shown in Figs. 8(c) and (d). This radial approached the GA at a heading of 53°T but changed to a heading of 41°T at a point 37 km from the GA and a bearing of 210°T . This heading was maintained for a short time until the aircraft reached a point approximately 18 km from the GA at a bearing of 204°T , where a heading of 43°T was assumed. This heading was maintained approximately throughout the remainder of this pass. The approach to the GA was therefore complicated by aircraft maneuvers; the data on this portion of the pass showed some interference behavior. On the departure from the GA, a $d^{-1/2}$ dependence was followed approximately. The field strength peak occurred simultaneously for both E and H at a distance of 36 km and a bearing of 54°T from the GA. However, at some other points, the E and H fields appeared to be 180° out of phase; the phase relationship between E and H was not constant over this pass. The field strength estimations shown in Fig. 1(a) suggested that strong directional effects should have been observed on this pass, and $d^{-1/2}$ field strength behavior was observed. The absence of data fit to a $d^{-1/2}$ dependence on the first half of the radial may be the result of the aircraft maneuvers, or it may be due to the fact that the first half of

the radial was less aligned with a strong-signal direction than the second half.

Third Radial—The measured field strength and calculated major component *vs* distance plots for the third radial are shown in Fig. 8(e) and (f). As may be seen from Fig. 2(e), this radial was also complicated by maneuvers in the area of the GA. This pass approached the GA at a heading of 158°T and apparently was one of the few radials that passed through the GA. The maneuvering began after the aircraft passed through the GA, and the subsequent data were difficult to analyze. After the aircraft reached a point at about 72 km and a bearing of 163°T from the GA, the field strength settled down and gradually decreased. It was at this point that the aircraft assumed its final heading of 156°T . A peak field ($E = 40$ db) at about 108 km and a bearing of 338°T from the GA was followed by a minimum field ($E = 31$ db) at about 56 km and the same bearing from the GA. The largest peak occurred at about 13 km and a bearing of 160°T from the GA when the aircraft was executing a maneuver; the E field at this point was about 45 db. During the maneuvering, the signal strength changed rapidly. The plot of Fig. 1(a) suggested that this radial should be close to a strong signal direction. However, no $d^{-1/2}$ behavior was observed. Very few interference effects were noted.

Fifth Flight Resume'

The double peaks on the first and third passes of the flight and the separation of the E and H major components on the first radial suggested a complicated antipodal situation. Definite conclusions regarding the motion of the antipode could not be reached. The maxima on the first and third passes occurred very close to each other in space, being separated by only about 6 km; however, the difference in magnitude was about 5 db. The second radial maximum occurred about 40 km from the positions of these peaks and was of approximately the same magnitude as the first pass peak. The first pass peak occurred at 1232 UT, the second pass peak occurred at 1406 UT, and the third pass maximum occurred at 1544 UT. The time separation of the peak occurrences was of the order of 1.5 hr. It would seem that perhaps the EA was somewhere eastward of the GA, judging from the positions of the various maxima.

Sixth Antipodal Flight

The sixth antipodal flight was performed on July 27, 1963, under conditions of local midnight at the antipode. The plot of the expected antipodal field strength patterns is shown in Fig. 1(b). A polar plot of the radials for this flight is shown in Fig. 2(f). The aircraft was in the vicinity of the GA over a period ranging from 2035 UT to about 0005 UT.

First Radial—The relevant data plots for this first radial are shown in Figs. 9(a) and (b). This radial missed the GA by about 25 km at a bearing of about 325°T . The aircraft entered the GA region from the northeast at a heading of about 232°T and switched to a heading of 227°T at a point 37 km distant from the GA and a bearing of 274°T . After this heading change, the field strengths appeared to obey the $d^{-1/2}$ relation, but before this alteration of the flight path no such behavior was very obvious. According to the polar plot of Fig. 1(b), the change in heading should have resulted in motion along a stronger signal direction, so perhaps this was the reason for the $d^{-1/2}$ behavior becoming more pronounced. An E field peak of about 53 db occurred at a point 58 km distant from the GA and a bearing of 255°T ; an H field peak occurred at a point 62 km from the GA and a bearing of 253°T . The E and H peaks were separated by about 5 km in space then. If the E and H peaks along a strong-signal direction were separated by a quarter of a wavelength, then the flight was making an angle of about 40° with a strong-signal direction. Thus, a strong-signal direction would be suggested, with a bearing of 267° , 187° , 87° , or 07°T . The polar plot of Fig. 1(b) suggested that the 267°T bearing was the most likely. There was some evidence of interference phenomena before the occurrence of the peak, but very little evidence of such effects after this peak. The plot of Fig. 1(b) predicted that this entire radial should have shown strong directional effects.

Second Radial—The measured field strength and calculated major component *vs* distance plots for the second radial are shown in Figs. 9(c) and (d), respectively. This radial approached the GA from the southwest at a heading of 330°T and passed this point at a distance of about 16 km and a bearing of 60°T ; at a point 20 km from the GA and a bearing of 20°T , the aircraft changed to a

new heading of 338°T , which was maintained until the aircraft was 120 km away from the GA. The signal levels appeared to build up gradually as the GA was approached and passed. An E field peak of 51.5 db occurred 20 km from the GA just as the aircraft was changing its heading; an H field minimum occurred simultaneously with this E field maximum. A second E field peak of approximately the same level occurred 65 km from the GA at a bearing of about 350°T . There were very few signs of interference effects and only slight indications of a $d^{-1/2}$ behavior, but, because of the large GA miss-distance, any conclusion regarding such behavior must be cautious. The field strength polar plot of Fig. 1(b) suggested that this radial would be along a weak-signal direction; conclusions about this point were not definite.

Third Radial—The pertinent data plots for the third radial are shown in Figs. 9(e) and (f). This radial entered the GA region at a heading of 109°T , but at a distance of 42 km and a bearing of 288°T from the GA, the aircraft changed to a 115°T heading. The GA was then passed at a distance of 5 km and a bearing of 200°T . The polar plot of Fig. 1(b) indicated that this pass should show definite strong-signal direction effects. Interference effects were evident, especially after the GA was passed, but no $d^{-1/2}$ behavior was definitely observed anywhere. As may be seen from Figs. 9(e) and (f), the field strengths maintained a fairly constant average level around 40 db after the aircraft passed the GA. A simultaneous peak of E and H occurred at approximately 54 km from the GA and a bearing of 288°T ; the E value at this point was about 57.5 db. If the first two radials did lie along strong-signal directions, then these signals might have produced the interference patterns seen on this radial without producing any $d^{-1/2}$ behavior.

Sixth Flight Resumé

Determination of the location of the EA from the data on this flight was extremely difficult; four widely scattered peaks of approximately the same magnitude were found on the three radials. However, the largest peak occurred on the last radial at a point west by northwest of the GA, so perhaps the EA was somewhere west of the GA. There was some indication of a $d^{-1/2}$ dependence in the field strength data on the first two passes, but conclu-

sions regarding such behavior must be cautiously drawn because these radials missed the GA (the origin of the data plots) by large distances. None of the radials clearly exhibited effects which were regarded as being characteristic of a strong-signal direction.

Seventh Antipodal Flight

The seventh and last antipodal flight was performed on July 28, 1963, around the time of local sunrise at the GA. The calculated field strength polar plot for antipodal sunrise is shown in Fig. 1(c). The flight radials are plotted in Fig. 2(g). The aircraft was in the antipodal region from about 0230 UT to about 0606 UT. Since local ionospheric sunrise occurred at about 0434 UT, the flight lasted from about 2 hr before sunrise to about 1.5 hr after sunrise.

First Radial—The measured field strength and calculated major component vs distance plots for the first radial are shown in Figs. 10(a) and (b). This radial approached the GA from the northeast at a heading of 226°T , which was maintained throughout the immediate vicinity of the antipode; the GA was passed at a distance of about 3 km and a bearing of about 315°T . The signal level was fairly constant around 53 db on the approach to the GA; then H and E maxima were recorded, respectively, at distances of 4 and 7 km and bearings of 270° and 250°T from the GA. These peaks were spatially separated by 4 km, or about a quarter of a wavelength. The E peak value was 62 db. The field strengths then decreased rapidly to minimal values at about 80 km and a bearing of 220°T from the GA for both E and H ; the E field here was 44 db. The field levels then increased gradually from this point. The field strengths apparently did not follow a $d^{-1/2}$ behavior on this radial, and the E and H fields appeared to be in phase throughout most of this radial. The polar plot of Fig. 1(c) suggested that this radial should show definite strong-signal direction effects, but apparently no such effects were definitely seen.

Second Radial—The second radial missed the GA by 20 km at a 77°T bearing. This pass maintained a heading of 348°T throughout the GA region. The measured field strength and calculated major component plots are shown in Figs. 10(c) and (d). The fields built up gradually on the approach to the GA, but a sharp dip in the E field occurred

about 21 km from the GA at a bearing of 62°T ; the field strength dropped from a previous level of 54 db to about 44 db. The previous level occurred just as the aircraft was passing the GA. After the minimum, the E field exhibited a peak of 60 db at a point 28 km from the GA and a bearing of 34°T . An H peak occurred about 38 km from the GA at a bearing of 20°T . The E and H peaks thus appeared to be separated by 13 km. The signal strengths decreased gradually from these peaks. There was some evidence of interference effects on the entire radial. The plot in Fig. 1(c) suggested that this radial should have been along a weak-signal direction. There was no evidence of any $d^{-1/2}$ behavior in the field strengths on this radial. The large dip in the E field in the vicinity of the GA could possibly have been a sunrise fade effect, since ionospheric sunrise occurred over the GA during this radial.

Third Radial — The third radial passed very close to the GA, apparently missing this point by a kilometer or less; by comparison with other radials in this experiment, this radial could be described as passing through the GA. An aircraft heading of 110°T was maintained throughout the antipodal vicinity. The measured field strength and calculated major component plots are given in Figs. 10(e) and (f). The field strength appeared to be at a peak value of approximately 53 db at a point about 160 km distant from the GA and a bearing of 290°T . The signal strength decreased to a minimal level, which occurred around 80 km from the GA at the same bearing, then an increase occurred again until a maximum signal level was reached at a point 11 km from the GA and a bearing of about 115°T . The E and H fields had coincident maxima at this point; the E field strength was about 66 db. The field strengths followed a $d^{-1/2}$ pattern very well in the interval from 160 km to 80 km west of the GA, but nowhere else did they appear to follow this behavior very closely. Interference effects could be noticed west of the GA, but after the aircraft passed through the GA, such effects were not so evident. The E and H fields appeared to be in phase with each other on this radial. The H field suffered deeper minima than the E field; separations of 14 db and 17 db were noted between adjacent maxima and minima. The largest separation noted in the E field data was about 11 db. The polar plot of Fig. 1(c) suggested that this radial should

be along a strong-signal direction; expected strong-signal direction behavior was noted only in the area far west of the GA. Ground sunrise occurred just as this radial was begun, so the antipodal field patterns were probably complicated by sunrise effects.

Seventh Flight Resumé'

The two peaks observed on both the first and third radials might have indicated that the EA was not a localized point, *i.e.*, antipodal effects might be observable over a wide area immediately surrounding the GA. These peaks could also have been the result of sunrise effects because the day-night discontinuity line moved through the antipodal region during this flight. The first and third passes recorded peaks of roughly the same magnitude close to the GA. Possibly these peaks could have represented the EA field strength at the times of their measurement, and the EA could have been close to the GA during this flight. If these two peaks nearest the GA on the first and third radials did represent the EA field strength, then the EA had apparently shifted about 17 km in a 110° direction in the 2 hr and 42 min interval between the occurrence of these peaks. The coincident appearance of the E and H field peaks on the third radial did not agree with the idealized antipodal models in which the maxima of E coincide with the minima of H , and vice versa. Such behavior could result, however, if the antipodal fields were due primarily to signals from predominantly one direction.

ANALYSES AND RESULTS

General Considerations

In discussing the antipodal experiment, there are several definitions that might be adopted. First of all, there is the geographic antipode, which is a geometric definition. Next, a definition of the electromagnetic antipode based on phase considerations could be made; for example, the area which is the limit of convergence of isophase contours might be defined as the electromagnetic antipode. The definition adopted for this report is that the electromagnetic antipode is the location of the maximum electric field strength observable in the antipodal region. Since the analysis deals

only with amplitude information, this definition seems the most appropriate. A further restriction might be that, at this point of maximum E field strength, the H field strength should be at a minimum value in order to agree with simple idealized theory. However, this restriction is not imposed since the real antipodal situation is not expected to fit too closely to the idealized case because of the nonuniformity of the earth-ionosphere waveguide, and also because the detection of the minimum of all the minima in the presence of noise is practically impossible.

In the following paragraphs, the results obtained from the experiment and the methods of analysis used to obtain the results will be discussed in some detail.

Field Strength Convergence

On every flight, an increase in magnitude of the field strength was observed as the aircraft approached the antipodal area. A convergence effect was therefore quite evident at the antipode of the NPM transmitting station. This result is in agreement with the results of earlier antipodal work, notably the 1962 joint experiment of NRL, NEL, and DECO Electronics, Inc. (5,6).

The maximum E field strength observed during the experiment occurred on the last flight; the value observed was 66 db above 1 $\mu\text{v/m}$, or 2.0 mv/m . This value is approximately the field strength expected for one mode over a daytime all-seawater path in an isotropic waveguide at a distance of about 3000 km from the same transmitter; the field strength of 2.0 mv/m near the antipode, which is approximately 20,000 km from the transmitter, does demonstrate the convergence effect.

Diurnal Variations

Prior to the actual performance of the experiment, attempts were made to calculate the antipodal field strength amplitudes and patterns at those times of the day at which it was planned to make the actual measurements. The basis for these calculations was the waveguide mode equation in modified form:

$$E = K + 10 \log P_r + \Lambda \\ - 10 \log f - 10 \log [a \sin (d/a)] \\ - \sum M \alpha_i d_i - \sum \Delta \alpha_g d_g$$

where

E = electric field intensity in decibels (db) relative to 1 $\mu\text{v/m}$

K = constant (db) dependent upon ionospheric height

P_r = radiated power of the transmitter in kilowatts (kw)

Λ = excitation factor (lumped loss) in db

f = transmitter frequency in kilocycles/second (kc/s)

a = earth radius in kilometers (km)

d = propagation path length in km

M = magnetic directional parameter (dimensionless)

α_i = attenuation rate in db per megameter (Mm) with an infinitely conducting earth and a constant ionospheric height

d_i = propagation path length in Mm for a given ionospheric height

$\Delta\alpha_g$ = additional attenuation rate in db/Mm for a given type of terrain with finite conductivity

d_g = propagation path length in Mm over a given type of terrain.

The values assumed for the above various propagation parameters are given below:

Additional Terrain Attenuation Rates

<i>Terrain</i>	$\Delta\alpha_g$ (db/Mm)
Sea water	0.0
Average land	1.0
Poor land	5.0
Arctic land	12.0
Greenland Icecap and Antarctica	24.0

*Ionospheric Attenuation Rates**

<i>Ionospheric Condition</i>	α_i (db/Mm)
Day ($h = 70$ km)	2.0
Night ($h = 90$ km)	1.0

Magnetic Directional Parameters

$$0.75 \leq M \leq 1.3$$

The M factor accounts for the nonreciprocal nature of vlf propagation along east-west directions in the earth-ionosphere cavity. This factor is a function of the angle between the earth's magnetic field and the propagation path and varies the ionospheric attenuation rate accordingly. The M values used in the antipodal calculations were averaged values taken over the entire propagation path. These values were taken from Wait (7). The values of Λ were taken from Wait and Spies (8).

It will be noted that the waveguide equation contains a singularity at the antipode because of the $-10 \log [a \sin (d/a)]$ term. This difficulty can be circumvented by calculating the field strength at a distance of 1 km from the antipode and then extrapolating to the antipode. As shown below, the $-10 \log [a \sin (d/a)]$ term vanishes if this approach is used.

At 1 km from the antipode, the propagation path length is $d = \pi a - 1$, so

$$\begin{aligned} a \sin\left(\frac{\pi a - 1}{a}\right) &= a \sin\left(\frac{1}{a}\right) \\ &\approx a \left\{ \frac{1}{a} - \left(\frac{1}{a}\right)^3 \dots \right\} \\ &\approx 1. \end{aligned}$$

Therefore,

$$-10 \log [a \sin(d/a)] \approx -10 \log 1 = 0.$$

The extrapolation to the antipode can be accomplished by using the expression for the envelope of the Bessel function, as given by Norton (3) for a single direction. This expression is

$$E = -15.964 - 10 \log (d/\lambda)$$

where E is the field strength in db relative to the field strength at the antipode, d is the distance in

km from the antipode, and λ is the wavelength of the signal in km. For the case where $d = 1$ km,

$$\begin{aligned} E &= -15.964 - 10 \log 1 + 10 \log \lambda \\ &= -15.964 + 10 \log \lambda \\ &= \text{constant (for a given } \lambda). \end{aligned}$$

Various propagation paths from the transmitter to the antipode were selected, and, for each path, an attempt was made to calculate the field strength from this path at a distance of 1 km from the antipode. For each path, the amount of each type of terrain crossed was considered, the percentage of each path in sunlight and in darkness was taken into account, and the loss for each path segment was estimated. The day-night transition lines were taken as sharp boundaries, and no discontinuity effects were considered. The calculated field strengths in millivolts per meter were then plotted on a polar plot centered at the antipode. A smooth curve was drawn through the field strength points, and the area enclosed by the curve was mechanically integrated. (This area represented an estimate of the energy arriving at the antipode.) This area was converted to an equivalent circular area of which the radius represented an effective field strength at 1 km from the antipode. The effective antipodal field strength was then obtained by extrapolation using the Bessel function envelope expression as given by Norton (3).

These calculations indicated that the sunrise fields should be highest, the sunset fields lowest, and the noon and midnight fields intermediate. The results are contained in Table 2 along with some measured peak fields at these various times of day. Polar plots of the calculated antipodal fields are given in Fig. 1.

As may be seen from Table 2, the measured peaks at these various times of day apparently followed the calculated diurnal pattern, although the measured field peaks were lower than those calculated. These differences may result from inaccurate calculations, or they may indicate that the aircraft never passed through the electromagnetic antipode, or they may result from combination of both conditions. The NEL ground station recordings near the antipode also showed the same diurnal behavior (9).

*Infinite ground conductivity.

TABLE 2
Antipodal Field Strengths

Local Ionospheric Condition	Computed E Field		Measured Peaks of E Field	
	(mv/m)	(db relative to $1 \mu\text{v/m}$)	(mv/m)	(db relative to $1 \mu\text{v/m}$)
Sunrise	4.23	72.5	2.00	66.0
			1.26	62.0
			1.19	61.5
Noon	2.00	66.0	1.19	61.5
			0.60	55.5
			0.53	54.5
Sunset	1.35	62.6	0.45	53.0
			0.38	51.5
			0.28	49.0
Midnight	1.84	65.3	0.75	57.5
			0.75	57.5
			0.60	55.5

The higher fields at local sunrise are apparently due to the nighttime, virtually all-seawater propagation path to the east from NPM through the Central American area. The path from the opposite direction is also virtually all seawater, but it is less favored at local sunrise because of its sunlit condition and because it is a propagation path to the west from the transmitter. Snyder *et al.* (9) have suggested that the difference in the amplitude of the sunrise and sunset fields may be due basically to the nonreciprocity (at vlf) of propagation to the east from the transmitter *vs* propagation to the west from the transmitter, since he feels that the sunset fields are due primarily to signals propagating to the west from NPM to the antipode. The other paths contain more attenuating land masses and are less favorable to propagation to the antipode than these two path sectors considered.

If Snyder's suggestion is correct, the sunrise and sunset fields should be primarily due to energy arriving from a single direction; therefore, the E and H fields should be in phase. The NEL ground site recordings indicated this behavior (9). On the first flight (which was also the first sunset flight), the E and H fields appeared to be out of phase near the time of local sunset, which occurred during the second radial (345° true heading). On the fifth flight (the second sunset flight), sunset occurred after the third radial (160° true heading);

the two fields appeared to be in phase *before*, and out of phase *after*, sunset. The E and H fields did not maintain a constant phase relationship relative to each other. On the third flight (the first sunrise flight), the E and H fields seemed to be in phase about the time of local sunrise, which occurred near the end of the third radial (151° true heading). The E and H fields also seemed to be in phase near the time of occurrence of sunrise on the seventh flight. Sunrise occurred on this flight near the end of the second radial (348° true heading).

The changing phase relationship of E and H on the fifth flight might have been the result of mode conversion effects as the day-night transition line moved through the antipodal region. The E and H fields apparently were out of phase just prior to sunrise, but they apparently were in phase during and just after sunrise on the seventh flight. This phenomenon again might be explainable in terms of mode conversion effects at the day-night discontinuity line.

The behavior of the E and H fields on the sunrise flights indicates that Snyder's suggestion may be correct, but the data from the sunset flights are not as conclusive. In this case, the NEL ground station data may prove to be more significant.

The calculated antipodal field strength polar plot in Fig. 1(a) for local sunset indicated a strong component arriving at the antipode from the east

and a stronger component from the southeast, but strong signals from the west and southwest were also predicted. This result did not quite agree with Snyder's suggestion, whereas the sunrise polar plot [Fig. 1(c)] showed virtually all of the energy coming from the west and southwest, which better agreed with Snyder's idea.

Distance Dependency of Antipodal Fields

As noted in the Introduction, simple antipodal theory predicts that the envelope of the field strength curves should vary as the inverse square root of distance d from the antipode, *i.e.*, $E = C d^{-1/2}$. For the idealized case, the major components, as defined in the Data Reduction section of this report, should also obey this relation. Hence, the major component *vs* distance from the geographic antipode plots were used to search for this type of behavior.

A plot of the function $f(d) = -10 \log |d|$ was constructed and applied to the major component plots to see if any sections of these plots fit this function. Several plots having portions that apparently obeyed this relation were found; the $f(d)$ function was then drawn on these plots, and the origin for $f(d)$ was indicated. As expected, the origin for $f(d)$ very seldom coincided with the origin (the geographic antipode) of the major component plots. The function $f(d)$ is plotted in Fig. 3.

All bearings from the antipode were not expected to show a $d^{-1/2}$ dependence due to the inhomogeneity of the earth-ionosphere waveguide. The strong-signal directions, such as the sector from the transmitter through Central America to the antipode, were expected to display $d^{-1/2}$ behavior because these sectors were very nearly homogeneous and more closely approximated the conditions of the idealized theory than the other paths. Figures 4(f) and 5(b) are examples of plots of data that were taken from flights along expected strong-signal bearings and showed the $d^{-1/2}$ behavior.

If the electromagnetic antipode, as defined in this report, were a single point, signals arriving from the less favorable propagation paths would have to increase faster than $d^{-1/2}$ in the antipodal area to attain the antipodal field strength level. Figure 5(f) shows a plot that built up to a peak more quickly than $d^{-1/2}$; this bearing was not expected to be a strong-signal direction.

If, on the other hand, one strong signal from a given bearing or sector predominated, an aircraft heading normal to this bearing would yield a fairly constant signal level. Behavior of this type is indicated by Figs. 6(d) and 7(d), although these flights were originally predicted to be parallel to a strong-signal direction, as discussed below. It may be noted that the results of the plots in Figs. 4(f), 5(b), and 5(f) agreed with the polar plot calculations in Figs. 1(a) and (b); the bearings indicated as strong-signal bearings by the polar plots showed expected strong-signal behavior on the flights, and the weak-signal bearing as indicated by the polar plot [Fig. 1(a)] did not show the $d^{-1/2}$ behavior expected of strong-signal bearings. However, as indicated by the polar plots in Figs. 1(c) and (d), the data plots in Figs. 6(d) and 7(d) should have shown strong-signal bearing behavior, but they did not. This disagreement indicates that the expected strong signal from the 200° to 240°T sector at the antipode was perhaps not present.

Several of the radials through the antipodal region showed a $d^{-1/2}$ behavior to some degree, and plots of the calculated major component data for these radials, along with the $f(d)$ curve, are shown in Figs. 4(b), (d), and (f); 5(b) and (d); 7(b) and (f); 8(b) and (d); 9(b), (d), and (f); and 10(b), (d), and (f). Very few of these plots obeyed the $d^{-1/2}$ relation over the whole radial; often only very small segments of the plots indicated this behavior. This behavior could result from the fact that the angular sector from which the observed signal was arriving became more homogeneous or less homogeneous as the aircraft moved through the antipodal area.

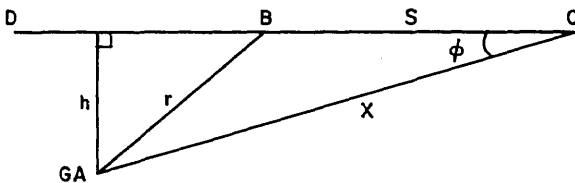
The concept of the angular sector over which the received signal arrives requires some elaboration. Briefly, this idea means that, because of the convergence of the various propagation paths as the antipode is approached, the received signal is the resultant of contributions from more and more paths as the observer moves closer and closer to the antipode; *i.e.*, as he moves closer to the antipode, he measures the resultant signal from a wider angular distribution of propagation paths. This idea has been given mathematical expression in the angle-of-acceptance concept as developed by D. D. Crombie (10).

The angle of acceptance θ is defined by

$$\cos (\theta/2) = 1 - \lambda/(2d)$$

where d is the distance from the antipode, and λ is the wavelength of the signal. Here it can be seen that as d gets smaller, θ gets larger until, at $d = \lambda/4$, $\theta = 2\pi$. Over a range of distances from the antipode where d is large and θ is small, the angular sector whose width is θ may be homogeneous; the signals arriving from this sector would then obey the $d^{-1/2}$ dependence. However, as d is reduced, θ would become larger such that the enclosed sector may not be homogeneous and the resultant field strength would depart from the $d^{-1/2}$ behavior over a given range of distance from the antipode. Thus, as a radial was flown through the antipodal region, only a small segment might be observed to follow the $d^{-1/2}$ pattern. This idea could also explain why different segments of the radial could show $d^{-1/2}$ field strength behavior, but the superimposed $f(d)$ curves on the data plots could have different origins.

It should be pointed out that sliding this $f(d)$ curve along the calculated major component plots to search for $d^{-1/2}$ behavior was not strictly correct. Since very few of the radials actually passed through the geographic antipode, two points B and C on the major component plots did not lie at the same bearing from the geographic antipode, and the distance BC was not the difference of the distances of B and C from the geographic antipode. However, if the radial passed very close to the geographic antipode and/or the distances considered were large, this method of searching for $d^{-1/2}$ behavior was permissible. The following diagram will illustrate the situation.



GA = geographic antipode

DC = a given pass near GA

h = distance of closest approach to GA

r = distance from GA to point B

x = distance from GA to another point (C)

ϕ = angle between x and CD

s = distance from B to C.

From the Cosine Law,

$$r^2 = s^2 + x^2 - 2sx \cos \phi,$$

or

$$s^2 + x^2 - r^2 = 2sx \cos \phi.$$

Now,

$$\sin \phi = h/x \text{ and } \cos \phi = [1 - \sin^2 \phi]^{1/2}$$

$$\cos \phi = [1 - (h/x)^2]^{1/2}.$$

By binomial expansion, $\cos \phi \approx 1 - (h/x)^2/2$. If h/x is very small, then $\cos \phi \approx 1$ and

$$s^2 + x^2 - r^2 \approx 2sx,$$

or rearranging,

$$s^2 - 2sx + x^2 = (s - x)^2 \approx r^2,$$

from which

$$(s - x) \approx \pm r$$

or

$$s \approx x \pm r.$$

Thus, for the condition $h/x \ll 1$, the distance between two points on the major component plots was approximately the difference of the distances of these points from the geographic antipode (origin), and the method of searching for $d^{-1/2}$ behavior via the $f(d)$ curve yielded negligible error. However, Figs. 4(d), 9(b), 9(d), and 10(d) were plots which indicated $d^{-1/2}$ behavior but which failed to satisfy the above condition at all times because of relatively large values of h .

Phase Relationships of E and H

The phase relationships as discussed in this section refer to the relative occurrence in time and space of the maxima and minima of E and H . According to simple antipodal theory, the maxima

of E should coincide with the minima of H , and vice versa; the phase relationship in this case would be a phase difference of 180° .

A definite pattern of phase behavior for the entire experiment was not discernible. For example, a phase difference of 180° was observed on the first flight, third radial, and the second flight, first radial, which were along strong-signal bearings. However, on the sixth flight, third radial, and the seventh flight, third radial, which were also along strong-signal bearings, the E and H fields appeared to be in phase. Also, on the third radial of the fourth flight, which was not expected to be along a strong-field direction, the E and H fields appeared to be 180° out of phase. All of the radials mentioned in this paragraph displayed $d^{-1/2}$ behavior to some degree. On some passes through the antipodal area, the phase relationship appeared to vary.

Perhaps, as suggested by Snyder, the cases where E and H were in phase indicated the reception of signals from a single propagation path only, and the cases where E and H were out of phase indicated a standing wave pattern resulting from signals from two or more paths. In any event, the phase behavior apparently did not follow a simple pattern. The changing phase behavior through the antipodal area may be attributable to inhomogeneities in the earth-ionosphere waveguide caused by differences in terrain conductivities and motion of the sunrise-sunset lines. Here again, the NEL ground station data may be more useful in determining any phase patterns that may exist.

Comparison of Flights During Similar Ionospheric Conditions

Flights taken at the same time of local day were compared for similarities in field strength behavior, repetition of antipodal patterns, and possible evidence of antipodal motion. The correspondence among the various flights was previously given in Table 1 and is used as the basis for comparison. As mentioned earlier, there was only one flight at local noon; hence, no comparison of local noon fields was possible.

Sunset Flights—The first and fifth flights were the two sunset flights, and polar plots of the radials of these two flights are given in Figs. 2(a) and (e).

The first flight, first radial, (approximately 225°T aircraft heading) and the fifth flight, second radial (approximately 45°T aircraft heading) were two corresponding passes showing little similarity in behavior of measured field strength vs distance from the geographic antipode; the data for these passes are shown in Figs. 4(a) and 8(c). If it were assumed that the peak field strengths on these radials represented similar points in the antipodal field patterns as measured on different days, some indication of antipodal motion was seen. This first flight peak (at 1510 UT) occurred at approximately 47 km and a bearing of 220°T from the position of the fifth flight peak (at 1406 UT); thus, if repetition of the antipodal patterns is assumed, a southwesterly drift with time is suggested. This first flight radial bypassed the geographic antipode at about 1408 UT; the fifth flight radial bypassed this point at about 1400 UT.

The first flight, second radial, and the fifth flight, third radial, showed little similarity in field strength patterns; these passes were difficult to compare because one of them went through the geographic antipode and the other missed this point by about 27 km. The field strength plots for these passes are given in Figs. 4(c) and 8(e). The second radial of the first flight had a 345°T direction and bypassed the geographic antipode at about 1640 UT; the third radial of the fifth flight had a direction of approximately 156°T and passed through the geographic antipode at about 1543 UT.

The first flight, third radial, and the fifth flight, first radial, had some similarity in field strength behavior; in the data plots shown in Figs. 4(e) and 8(a), the peaks did not appear to be shifted relative to each other. The flight patterns were fairly similar; however, the first flight radial bypassed the geographic antipode at about 1802 UT (aircraft heading of approximately 105°T), and the fifth flight radial bypassed this point at about 1234 UT (aircraft heading of approximately 290°T). This result may have indicated repetition of the antipodal patterns, but it showed nothing about the motion of the electromagnetic antipode.

Midnight Fields—The second flight and the sixth flight were the two midnight flights; polar plots of these flights are given in Figs. 2(b) and (f).

The second flight, first radial (in approximately a 283°T direction) and the sixth flight, third radial (in approximately a 115°T direction) displayed

doubtful similarity in measured field strength *vs* distance plots, as shown in Figs. 5(a) and 9(e). This second flight radial bypassed the geographic antipode at about 1953 UT; the sixth flight radial bypassed this point at about 2336 UT and on the opposite side from the second flight radial. According to the calculated field strength polar plot in Fig. 1(b), both of these passes should have been along a strong-signal direction. Although these radials passed on opposite sides of the geographic antipode, neither of them missed this point by a large margin. On this basis, some similarity should have been noted. However, the lack of similarity can possibly be accounted for by the 3 hr and 43 min difference in antipodal passing times. In that interval, propagation conditions could change enough to destroy any similarity that might have existed. The peak appeared to have shifted by approximately 32 km and in a 275°T direction from the second flight pass to the sixth flight pass.

The measured field strength *vs* distance plots for the second radial of the second flight and the first radial of the sixth flight are shown in Figs. 5(c) and 9(a). These passes had no similarity in field strength behavior. This second flight radial bypassed the geographic antipode at about 2124 UT (aircraft heading approximately 035°T), and the sixth flight radial bypassed this point at about 2056 UT (aircraft heading approximately 232°T); thus, these passes occurred at approximately the same time of day. They passed the geographic antipode on the same side, but the sixth flight radial missed this point by approximately 25 km, whereas the second flight radial missed this point by only about 4 km. This lack of similarity may be due to the amount of aircraft maneuvering on the second flight. Both plots show field strength levels to be fairly constant; such behavior could result from aircraft flight normal to a strong-signal direction and would make similarity of field strength pattern more difficult to detect.

The second flight, third radial, bypassed the geographic antipode at approximately 2310 UT at an aircraft heading of about 140°T; the sixth flight, second radial, bypassed this point at approximately 2228 UT at an aircraft heading of 330°T. The measured field strength *vs* distance plots are shown in Figs. 5(e) and 9(c). These passes missed the geographic antipode on opposite sides by distances of 12 and 16 km, respectively; the directions of the flight paths differed by more

than 20° for major portions of these radials, *i.e.*, the two passes missed being parallel by more than 20°. The lack of similarity in the passes themselves and the scarcity of data points on the sixth flight radial did not allow a definite conclusion regarding the similarity of behavior of the measured field strength plots.

Sunrise Flights – The third flight and the seventh flight were performed around the time of local sunrise at the antipode; polar plots of these flights are shown in Figs. 2(c) and (g).

The measured field strength *vs* distance plots for the third flight, first radial, and the seventh flight, third radial, are shown in Figs. 6(a) and 10(e). The third flight, first radial, bypassed the geographic antipode at approximately 0108 UT in a direction of 290°T; the seventh flight, third radial, bypassed this point at approximately 0537 UT in a direction of 110°T. These two passes showed some similarity in field strength behavior. The maximum field strength recorded on this seventh flight pass occurred at approximately 64 km and a 110°T bearing from the position of a similar peak on the third flight radial; the third flight pass occurred before sunrise, and the seventh flight pass occurred after sunrise, so perhaps an easterly shift of the electromagnetic antipode during the sunrise period is indicated.

The third flight, second radial, bypassed the geographic antipode at approximately 0232 UT in a 039°T direction; the seventh flight, first radial, passed this point at approximately 0257 UT in a 226°T direction. The measured field strength *vs* distance plots for these radials are shown in Figs. 6(c) and 10(a). Comparison of these two passes was uncertain due to the fact that they passed the geographic antipode on opposite sides, and the third flight radial missed this point by about 26 km; no conclusions regarding similarity were obtained.

Similar difficulties arose in comparing the third radial of the third flight and the second radial of the seventh flight. These radials passed the geographic antipode on opposite sides, with the seventh flight radial missing this point by about 20 km; moreover, the flight paths missed being parallel by about 17°. The third flight radial passed the geographic antipode at approximately 0407 UT in a 151°T direction; the seventh flight radial passed this point at approximately 0413 UT in a 348°T direction. The measured field strength

vs distance plots for these two radials are shown in Figs. 6(e) and 10(c). While keeping these differences in the two radials in mind, it could be noted that there was no apparent relative shift in the field strength *vs* distance patterns. Since these radials occurred at approximately the same time of day, perhaps there was some indication of day-to-day repetition of antipodal field patterns. However, this conclusion must necessarily be weak. The polar plot in Fig. 1(c) and the similar times of occurrence of the passes indicate that perhaps some similarity between the two field strength patterns should have been expected.

The comparisons in this section of the report are not offered as definite conclusions, but only as suggestions of possibilities that may be found in the actual situation. Here again the navigational difficulties have arisen to make valid comparisons and conclusions difficult to achieve.

Comparison of Similar Radials at Different Ionospheric Conditions

A comparison of similar radials flown at different day and night conditions along the various propagation paths was attempted, and a few similarities in the field strength behavior were noted.

The first flight, second radial, [sunset—see Figs. 2(a) and 4(c)], the third flight, third radial, [sunrise—see Figs. 2(c) and 6(e)], and the fourth flight, third radial, [noon—see Figs. 2(d) and 7(e)] showed some similarity in the field strength *vs* distance behavior. The third and fourth flight radials came very close to the geographic antipode, but the first flight radial missed this reference point by about 26 km; therefore, a comparison of the first flight radial with the other two radials was less reliable. The field strength peak on the fourth flight radial was shifted by approximately 30 km at a 130°T bearing relative to the position of the field strength peak on the third flight radial. The third flight radial peak occurred at 0954 UT. From the calculated polar plots for sunrise and noon [Figs. 1(c) and (d)], it may be seen that a stronger signal was expected at the antipode from the westerly sector at sunrise than at noon; also, at noon, larger contributions were expected from bearings of 095°T and 148°T than at sunrise, when most of the energy was expected to arrive from westerly bearings.

Thus, it might be anticipated that the electromagnetic antipode would be further west at sunrise than at noon; this fact could perhaps explain the shift in position between the peak field strengths on these third and fourth flight radials.

The first flight, third radial, [sunset—see Figs. 2(a) and 4(e)] showed fair similarity to the seventh flight, third radial, [sunrise—see Figs. 2(g) and 10(e)] and some similarity to the third flight, first radial, [sunrise—see Figs. 2(c) and 6(a)] in the field strength *vs* distance behavior, especially in the region east of the geographic antipode. West of this point, the third flight path had a different direction from the direction of these other two passes; therefore, comparison was more difficult for that portion of the third flight pass. The peak field strength on the first flight radial occurred at 1754 UT, and the peak strength on the seventh flight radial occurred at 0539 UT. The position of the seventh flight radial peak was approximately 52 km at a 100°T bearing from the position of the first flight radial peak. From the predicted field strength polar plots for sunset and sunrise [Figs. 1(a) and (c)], it might be expected that the electromagnetic antipode would be further east at sunset than at sunrise because of lower contributions from western sectors and higher contributions from easterly and south-easterly sectors at sunset than at sunrise. However, at both sunrise and sunset, the antipodal fields are probably subject to mode conversion effects due to the day-night transition line and its motion. These effects may explain why the seventh flight radial peak occurred eastward for the first flight radial peak. As will be pointed out later in this report, the seventh flight, third radial, had two distinct field strength peaks which again could possibly be explained as the result of mode conversion effects.

These comparisons, like those of the preceding section, are not offered as conclusions but as suggestions; they merely represent attempts to gain some idea of the relative antipodal situations at various times of day.

Departures from Simple Theory

A couple of items of interest concerning the data were noticed in the analysis; these were items

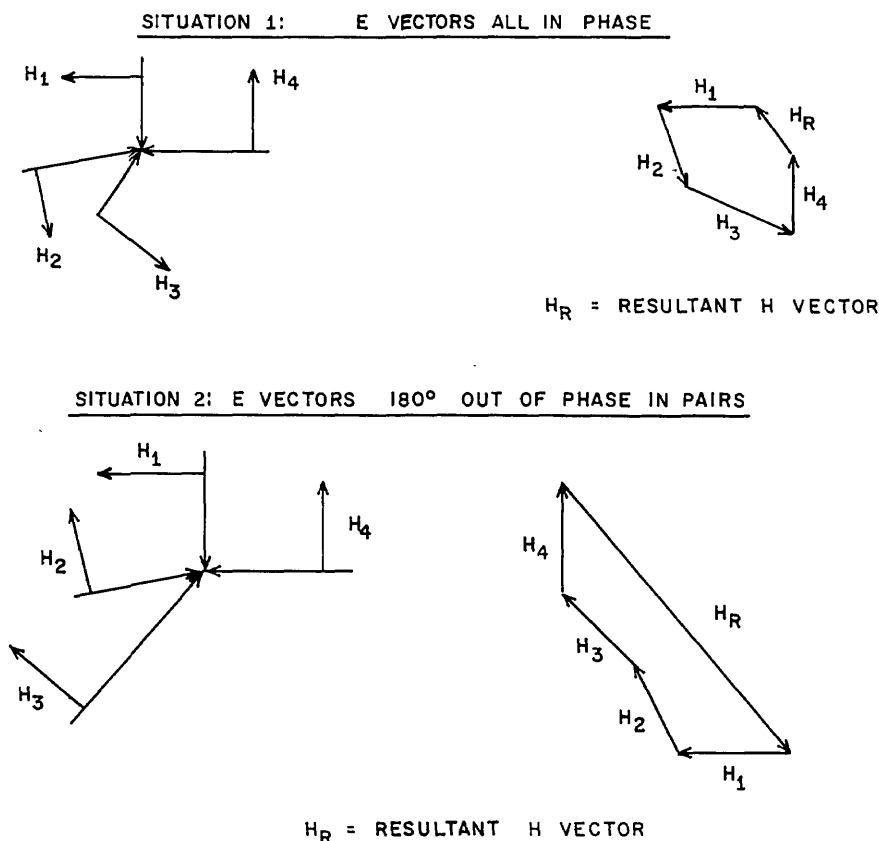
that represented deviations from the predictions of simple ideas about the antipode.

The first item concerned the separation of the major components of the E and H fields. As explained earlier, the major components were computed quantities based on two interfering signals; in the case of two such signals, or for the idealized antipode, the major components of E and H should vary in the same way. However, on some passes, the E and H major components followed different patterns. This type of behavior was particularly noticeable on the first radial of the fifth flight; the major component plot of this data is given in Fig. 8(b). This phenomenon might have been indicative of a somewhat complicated interference pattern.

The calculated field strength polar plot for sunset at the antipode [Fig. 1(a)] indicated about four strong-signal directions. A complicated interference pattern could result from such a situation. For example, consider the following simplified situations of four equal-amplitude signals arriving

from four different directions. The signals are all vertically polarized. The E vectors are normal to the plane of the paper. The numbered arrows are the H vectors, and the other arrows indicate the direction of propagation. If the field is measured at points where situations 1 and 2 exist, and at intermediate points, the phases of the resultant E and H fields may vary in some complicated way, and the calculated major components of E and H may possibly not vary in the same manner.

The second item of interest concerned the appearance of two peaks in the major components on some of the radials. This phenomenon was quite evident on the first and third radials of the seventh flight and on the second radial of the fourth flight. Plots of these effects are shown in Figs. 10(b), 10(f), and 7(d), respectively. According to the calculated polar plots of field strength, these radials were all expected to be parallel to the directions of arrival of strong signals. These results could have indicated that a single antipode, as defined in this report, did not exist at these



times of day, specifically just around sunrise and at local noon. These phenomena could also have indicated that the antipode is not a localized point as in the simpler models, but may be spread out, *i.e.*, antipodal effects may be observed over a large area immediately around the geographic antipode. It was also possible that the aircraft missed the electromagnetic antipode but passed through two field strength maxima in the antipodal vicinity. The two peaks on the seventh flight radials at sunrise could possibly arise from transition effects as the sunrise line moved through the antipodal region, producing mode conversion effects and additional interference phenomena in the antipodal field patterns.

CONCLUSIONS

When actual worldwide propagation conditions are considered, differences between the real antipodal situation and the idealized models (assumed in this report) should not be too surprising. Because of such factors as the differences in day and night ionospheric heights and attenuations, the different attenuation rates for various terrains, and the nonreciprocity of east-to-west *vs* west-to-east propagation, the earth-ionosphere cavity is certainly an inhomogeneous, anisotropic waveguide. Since the sunrise and sunset lines are continually moving across the face of the globe, conditions along the various propagation paths to the antipode are continually changing. Thus, it would seem that a nonstatic antipodal situation is generated in which the field strengths, phases, and field patterns are variable with time. This condition contributes to the complexity of the data analysis.

The analysis of the data is further complicated by any navigational difficulties encountered. For example, for the data contained in this report, uncertainties in aircraft position very probably contribute to errors in the plots of field strength *vs* distance, and in the results derived from these plots.

In spite of these difficulties, some conclusions regarding the antipodal situation are possible. Definite convergence effects, such as signal strength increases and interference phenomena, are observable on every flight; several radials flown through the antipodal area have portions

in which the $d^{-1/2}$ behavior as predicted by Norton (3) is observed. Pre-experiment calculations of the azimuthal dependence and amplitudes of the signals for the various times of day are in fair agreement with the observed diurnal variations of field strength and the observed directions of arrival for strong signals, although the observed field strengths are lower than those predicted. This result is another verification of the waveguide mode equation. The antipodal calculations used were made in March 1963; if more recent values of the propagation parameters had been used, the calculations would probably yield different values closer in agreement to experimentally measured results.

It is not possible to conclusively state that the aircraft ever actually passed through the electromagnetic antipode; this fact would also account for some of the disparity between the measured and the calculated field strength peaks. The peak value (66 db above 1 microvolt per meter) observed on the third radial of the last flight may have actually been the electromagnetic antipode as defined in this report, but this cannot be definitely stated.

The appearance of multiple peaks in the major components on some radials and the separation of the E and H major components on various radials represent deviations from the simpler idealized models of the antipode. These effects suggest that the real antipode is more complex than the simple models. The multiple peaks indicate that the electromagnetic antipode is perhaps not a localized point; antipodal effects might be measurable over a large region immediately surrounding the geographic antipode.

It is felt that the aircraft data are not sufficiently good to permit calculations of attenuation rates. In performing such calculations, the fact that the signals may be arriving over multiple paths instead of a single path must be considered; the inhomogeneities in the paths and the differences in the paths for different angular sectors at the antipode may cause diffraction effects. These diffraction effects and the interference of multiple signals make attenuation rate calculations difficult.

Comparisons of peak signal strengths obtained on similar radials, flown under similar propagation conditions and under different propagation conditions, and a study of the individual flights give some indications that the position of the

electromagnetic antipode varies with time. For example, at sunset a southwesterly drift of similar peaks is indicated; at midnight, the motion seems more westerly; at sunrise, the movement appears to be easterly or northeasterly; at noon, a drift direction cannot be ascertained, but in the period from sunrise to noon, an easterly motion seems to occur. Due to the changing propagation conditions, a movement of the electromagnetic antipode is expected. Since it is not certain that the aircraft ever passed through the electromagnetic antipode, it is not possible to describe the path or extent of this motion. The assumed movements of these similar peaks are shown in the polar plot in Fig. 11.

It would appear that an antipodal experiment of this kind, with data gathered from a mobile receiver, contains too many indeterminate variables. Continuous monitoring of the antipodal signals from ground-based receiving sites, of which the positions relative to the geographic antipode are known, would probably yield more meaningful data. This was the approach taken by NEL in their participation in this experiment. It is possible that when the NRL aircraft data and the NEL data—both from the aircraft and the ground sites—are combined, more significant conclusions concerning the NPM antipode can be reached.

ACKNOWLEDGMENTS

The author wishes to thank the officers and crew of the aircraft, commanded by Cdr A. V. McPhillips, for their cooperation in this project. The assistance of L. H. Nelson and M. C. Kronschnabel of the Radio Corporation of America in the collection of the data is gratefully

acknowledged. The author also wishes to thank his colleagues, W. E. Garner, F. J. Rhoads, and R. L. Schauer, for valuable assistance and discussions in the processing and analysis of the data.

REFERENCES

1. Wait, J.R., "Terrestrial Propagation of Very-Low-Frequency Radio Waves," *J. Res. Natl. Bur. Std., D.* **64D**(No. 2):153-201 (1960)
2. Norton, K.A., "Transmission Loss in Radio Propagation-II," NBS Technical Note No. 12, June 1959
3. Crombie, D.D., "Differences Between the East-West and West-East Propagation of VLF Signals Over Long Distances," *J. Atmospheric Terrest. Phys.* **12**:110 (1958)
4. Round, H.J., Eckersley, T.L., Tremellen, K., and Lunnon, F.C., "Report on Measurements Made on Signal Strength at Great Distances During 1922 and 1923 by an Expedition Sent to Australia," *J. Inst. Elec. Engrs. (London)* **63**:933-1011 (1925)
5. Garner, W.E., and Rhoads, F.J., (U.S. Naval Research Laboratory), Bickel, J.E., and Plush, R.W., "Measured Amplitude and Phase of the Antipodal Fields of a VLF Transmitter," paper presented at the 1962 Fall URSI meeting, October 15-17, 1962, Ottawa, Canada
6. Garner, W.E., and Rhoads, F.J., "Antipodal Effects in VLF Wave Propagation," Rept. NRL Prog., pp. 17-19, Aug. 1962
7. Wait, J.R., "A New Approach to the Mode Theory of VLF Propagation," *J. Res. Natl. Bur. Std., D.* **65D**(No. 1):37-46 (1961)
8. Wait, J.R., and Spies, K.P., "Height-Gain for VLF Radio Waves." *J. Res. Natl. Bur. Std., D.* **67D**(No. 2):183-187 (1963)
9. Snyder, F.P., Bickel, J.E., and Paulson, M.R., "Antipodal-Field Measurements of VLF Transmitter NPM at Stationary Sites," NEL Report 1294, May 27, 1965
10. Crombie, D.D., (Institute for Telecommunication Sciences and Aeronomy, Boulder, Colo.) "On the Electric Field of a VLF Transmitter Near its Antipodes," paper presented at the 1962 Fall URSI meeting, October 15-17, 1962, Ottawa, Canada

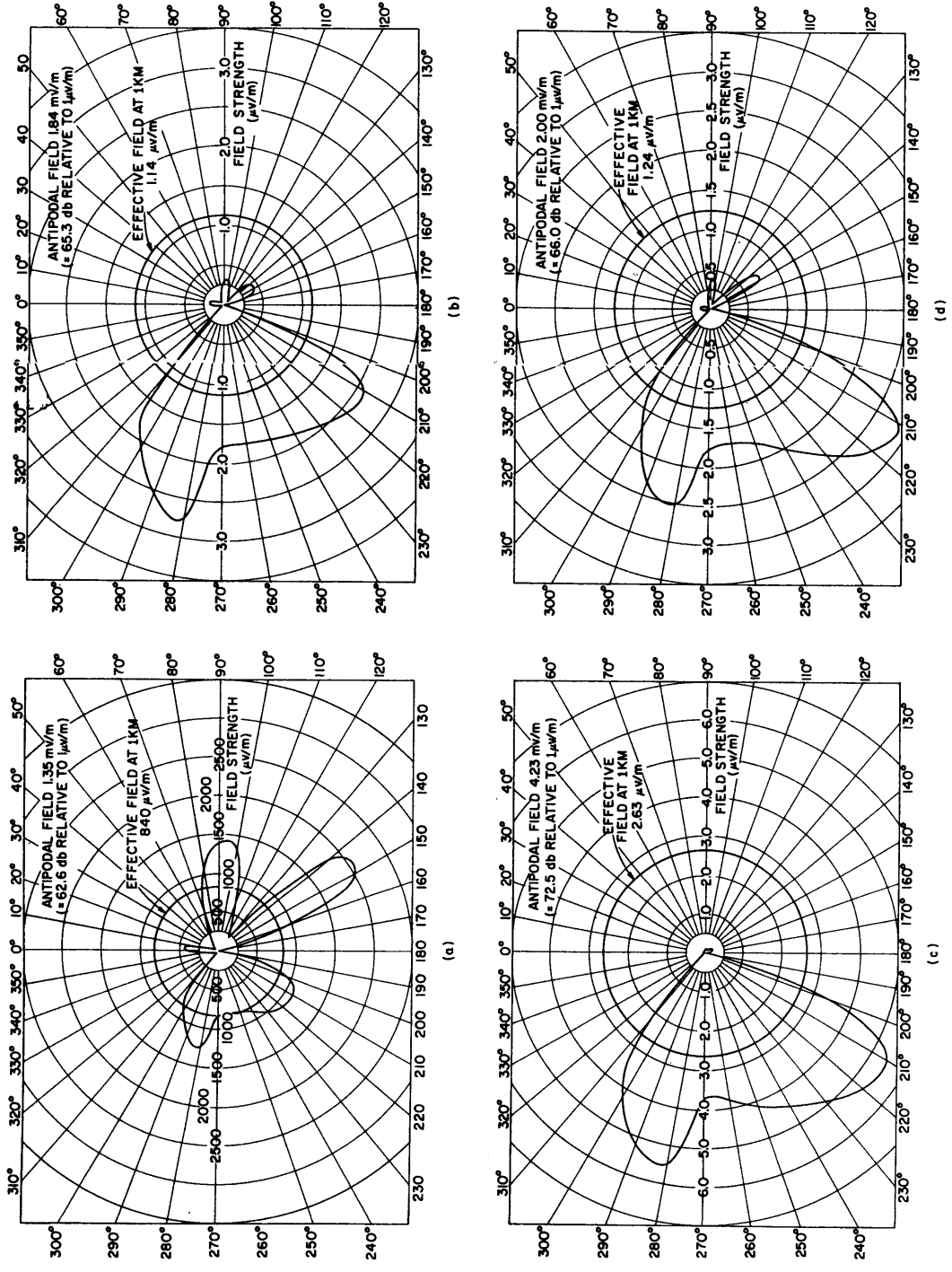


Fig. 1 - Azimuthal plots of the calculated field strengths at a distance of 1 km from the antipode of station NPM for the month of March. The calculations are based on ionospheric conditions that exist at (a) local sunset, (b) local midnight, (c) local sunrise, and (d) local noon. (Correction for antipodal field strength: add 4.16 db or $\times 1.61$.)

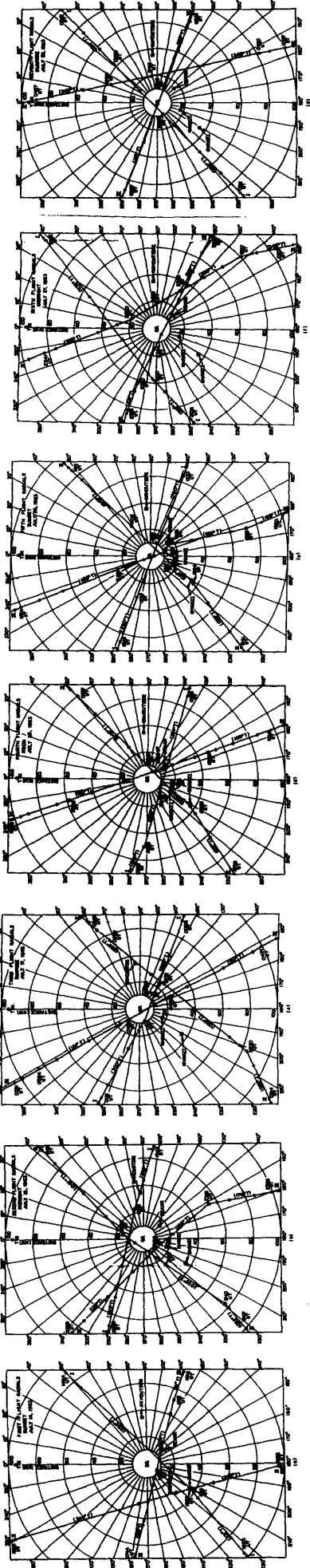


Fig. 2 - Polar plots of the radials traversed on each of the seven flights in the vicinity of the radar station. The radial paths and geographic headings and the time at various locations are indicated for each of the flights.

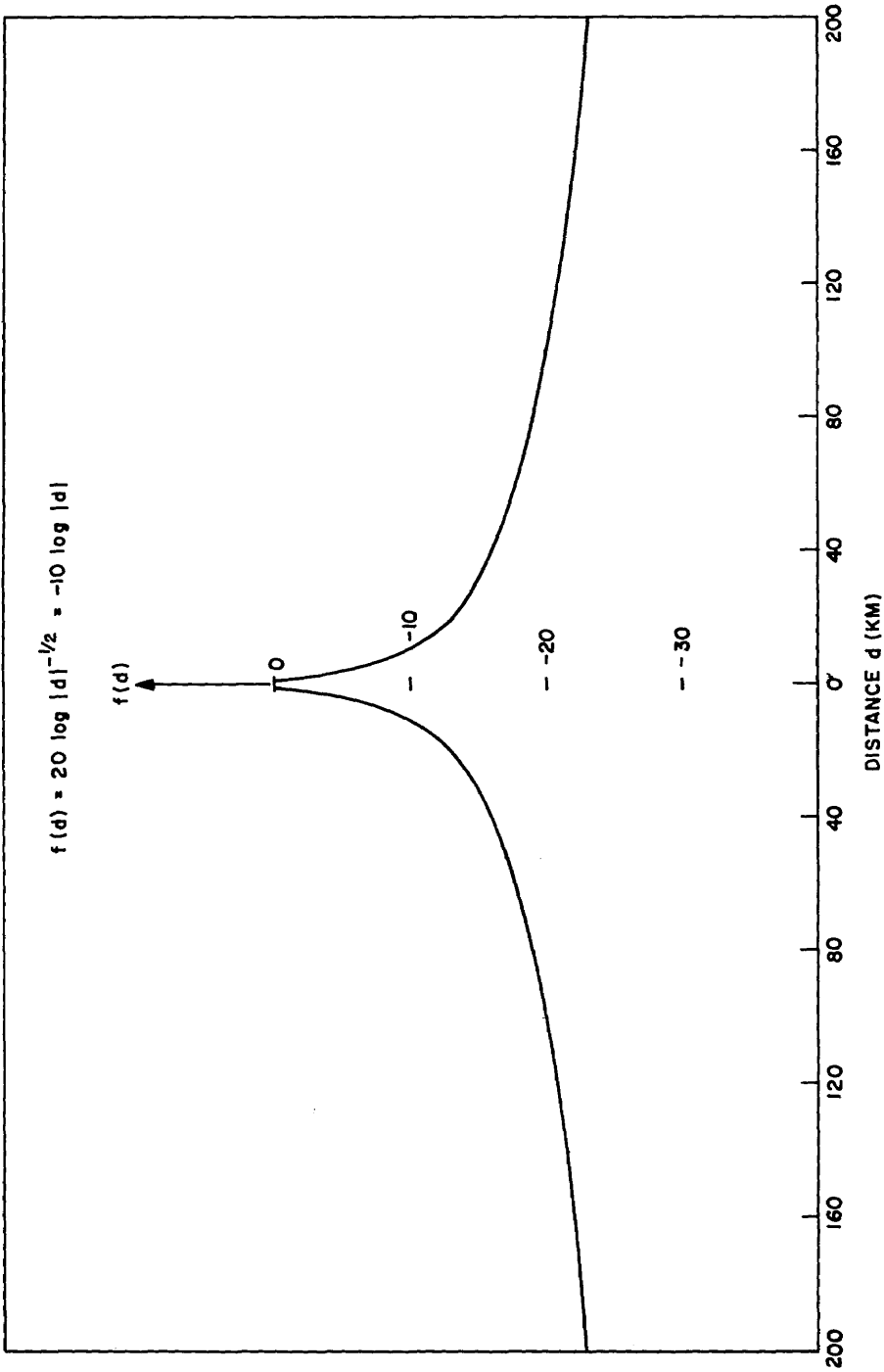


Fig. 3 - Plot of the function $f(d) = -10 \log |d|$ vs d

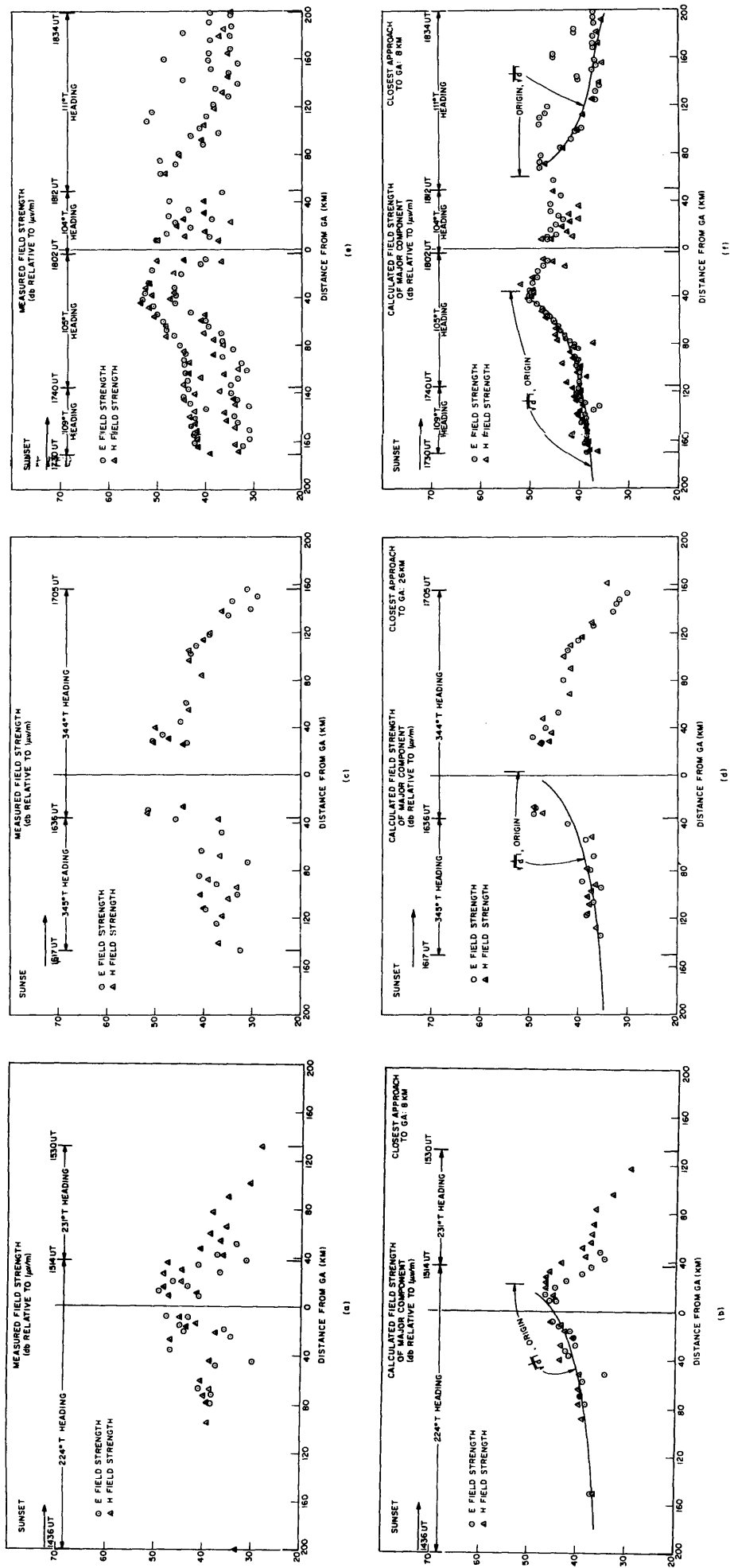


Fig. 4 — Measured field strengths vs distance from the geographic antipode (GA) for (a) the first radial, (c) the second radial, and (e) the third radial of the first flight. The calculated field strength major components vs distance from the geographic antipode are shown for (b) the first radial, (d) the second radial, and (f) the third radial of the first flight. The time at turning points and the aircraft headings between points are indicated.

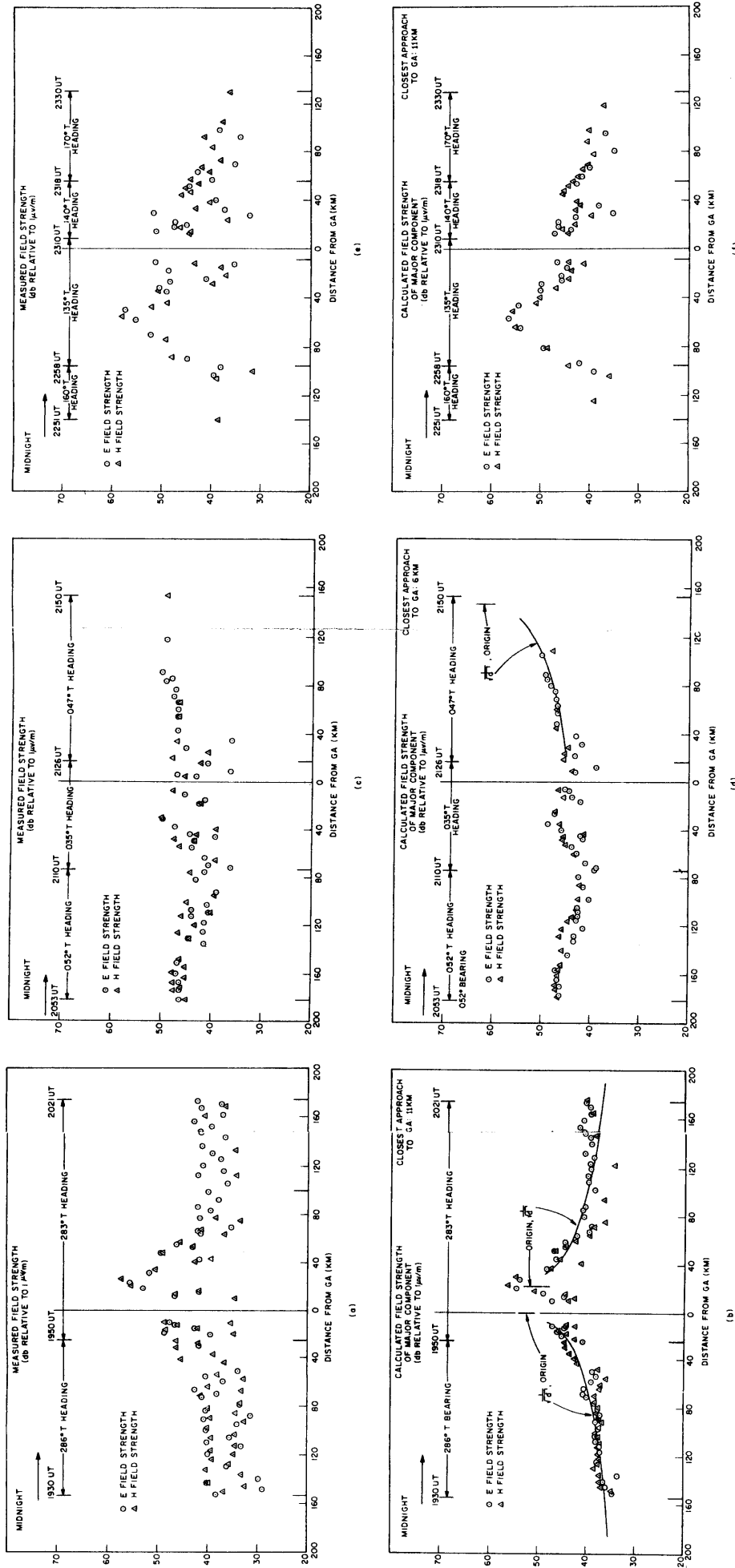


Fig. 5 - Measured field strengths vs distance from the geographic antipode (GA) for (a) the first radial, (c) the second radial, and (e) the third radial of the second flight. The calculated field strength major components vs distance from the geographic antipode are shown for (b) the first radial, (d) the second radial, and (f) the third radial of the second flight. The time at turning points and the aircraft headings between points are indicated.

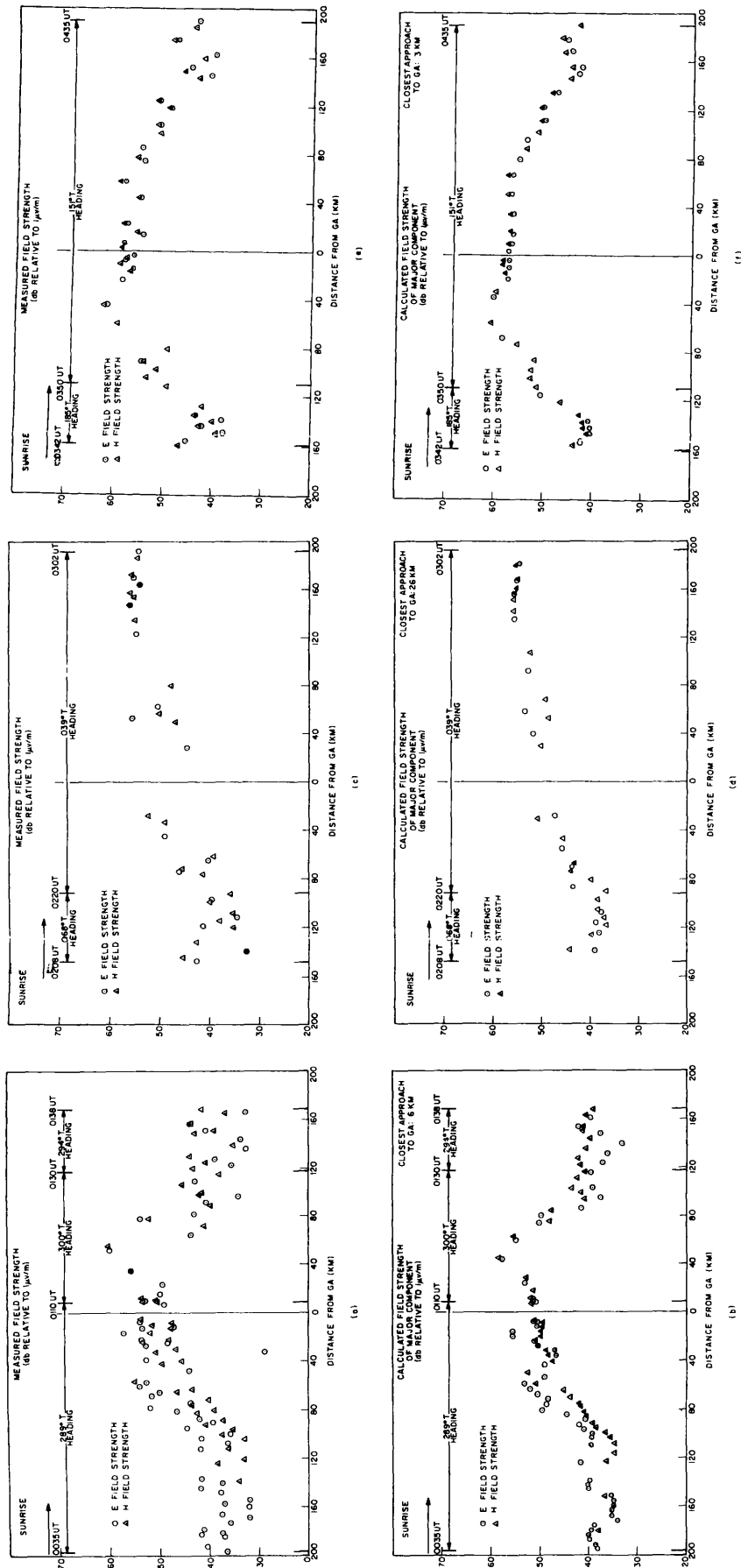


Fig. 6 - Measured field strengths vs distance from the geographic antipode (GA) for (a) the first radial, (c) the second radial, and (e) the third radial of the third flight. The calculated field strength major components vs distance from the geographic antipode are shown for (b) the first radial, (d) the second radial, and (f) the third radial of the third flight. The time at turning points and the aircraft headings between points are indicated.

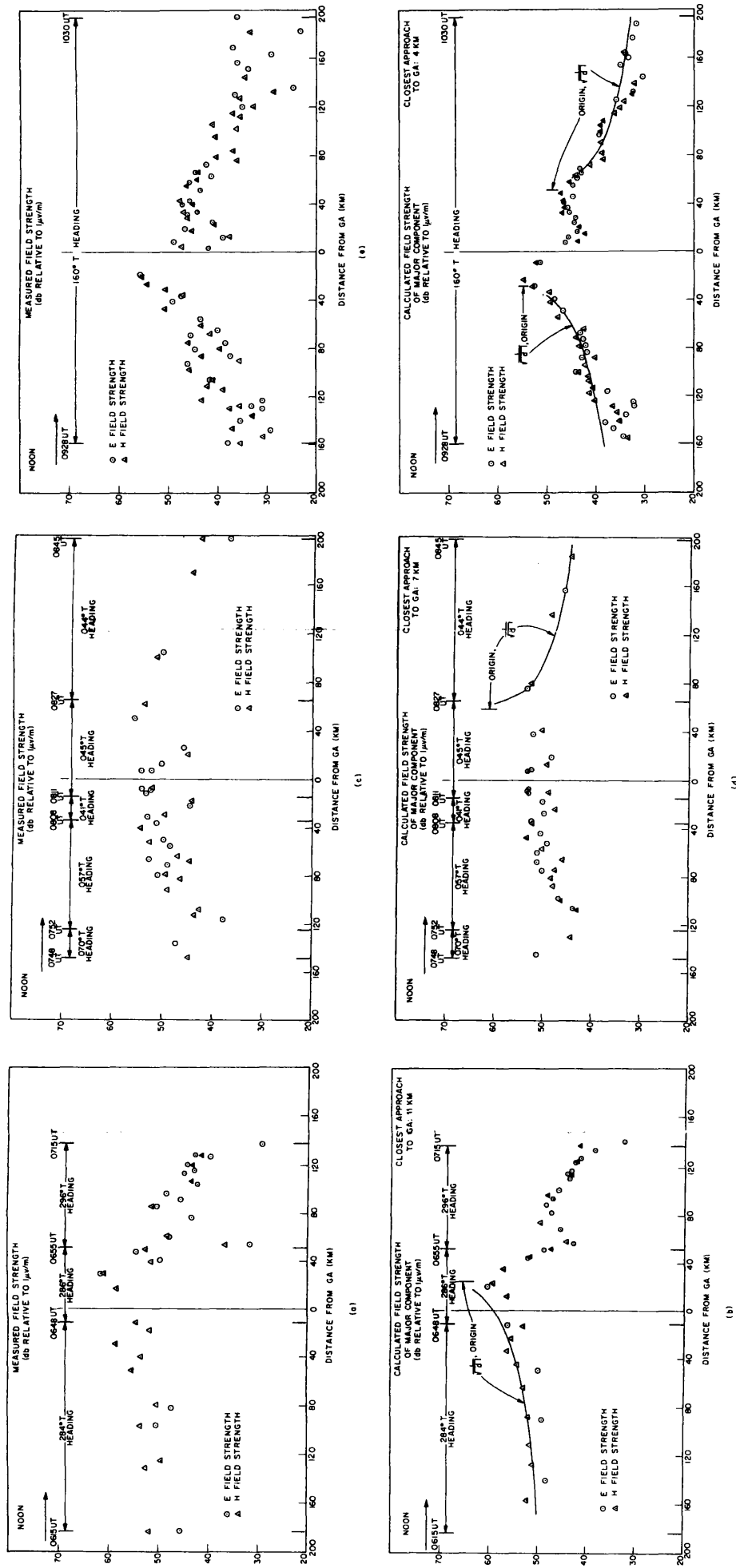


Fig. 7 - Measured field strengths vs distance from the geographic antipode (GA) for (a) the first radial, (c) the second radial, and (e) the third radial of the fourth flight. The calculated field strength major components vs distance from the geographic antipode are shown for (b) the first radial, (d) the second radial, and (f) the third radial of the fourth flight. The time at turning points and the aircraft headings between points are indicated.

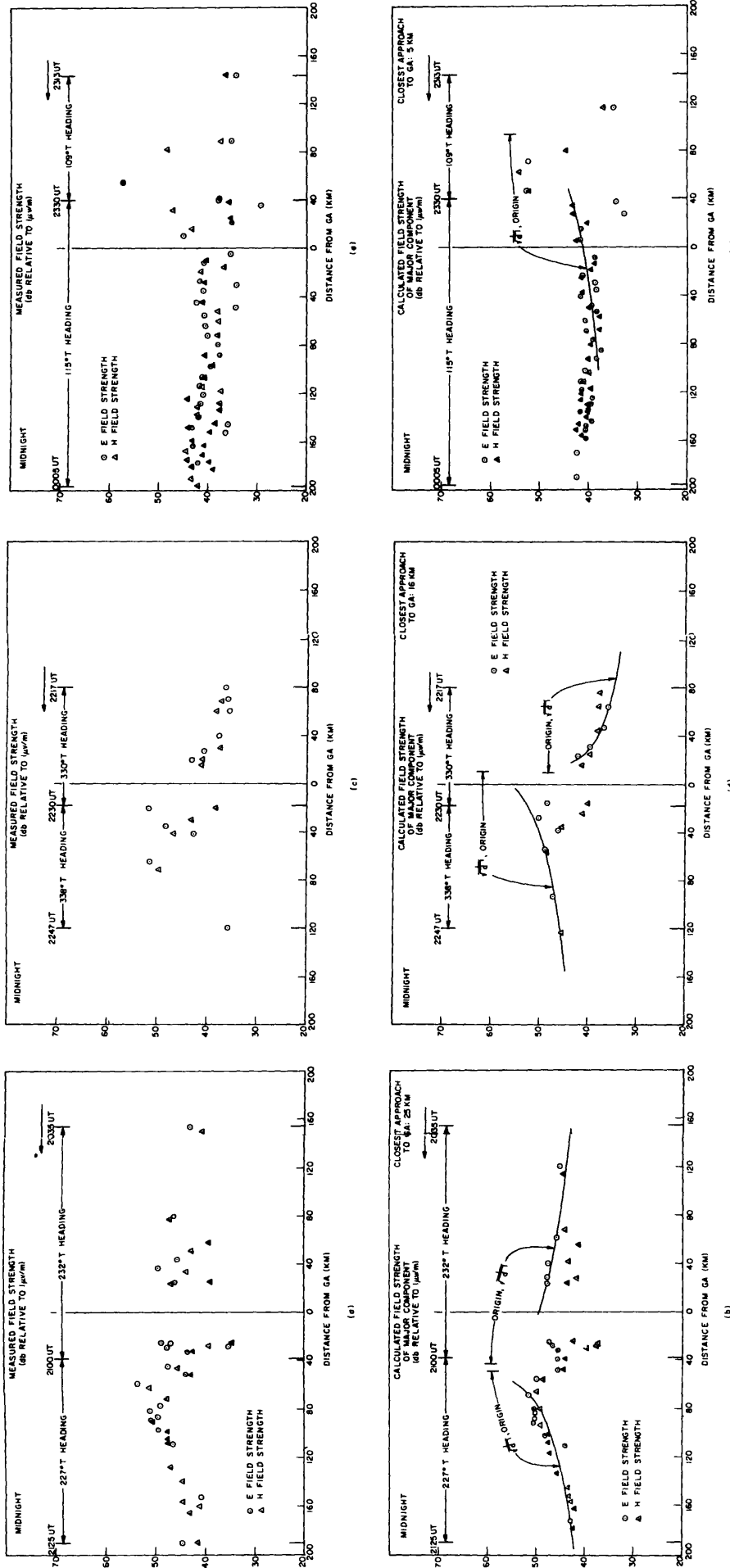


Fig. 9 - Measured field strengths vs distance from the geographic antenna (GA) for (a) the first radial, (c) the second radial, and (e) the third radial of the sixth flight. The calculated field strength major components vs distance from the geographic antenna are shown for (b) the first radial, (d) the second radial, and (f) the third radial of the sixth flight. The time at turning points and the aircraft headings between points are indicated.

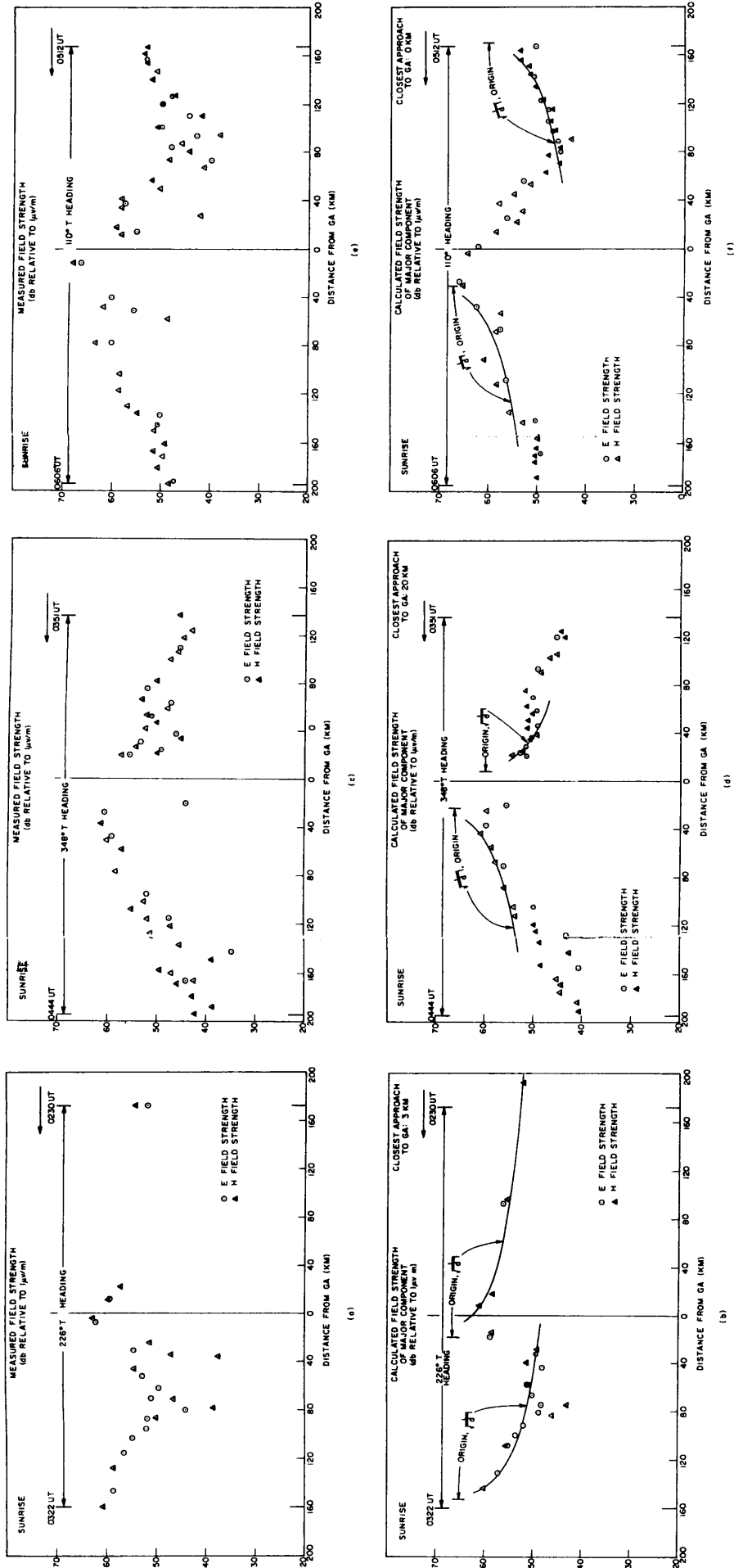


Fig. 10 - Measured field strengths vs distance from the geographic antipode (GA) for (a) the first radial, (c) the second radial, and (e) the third radial of the seventh flight. The calculated field strength major components vs distance from the geographic antipode are shown for (b) the first radial, (d) the second radial, and (f) the third radial of the seventh flight. The time at turning points and the aircraft headings between points are indicated.

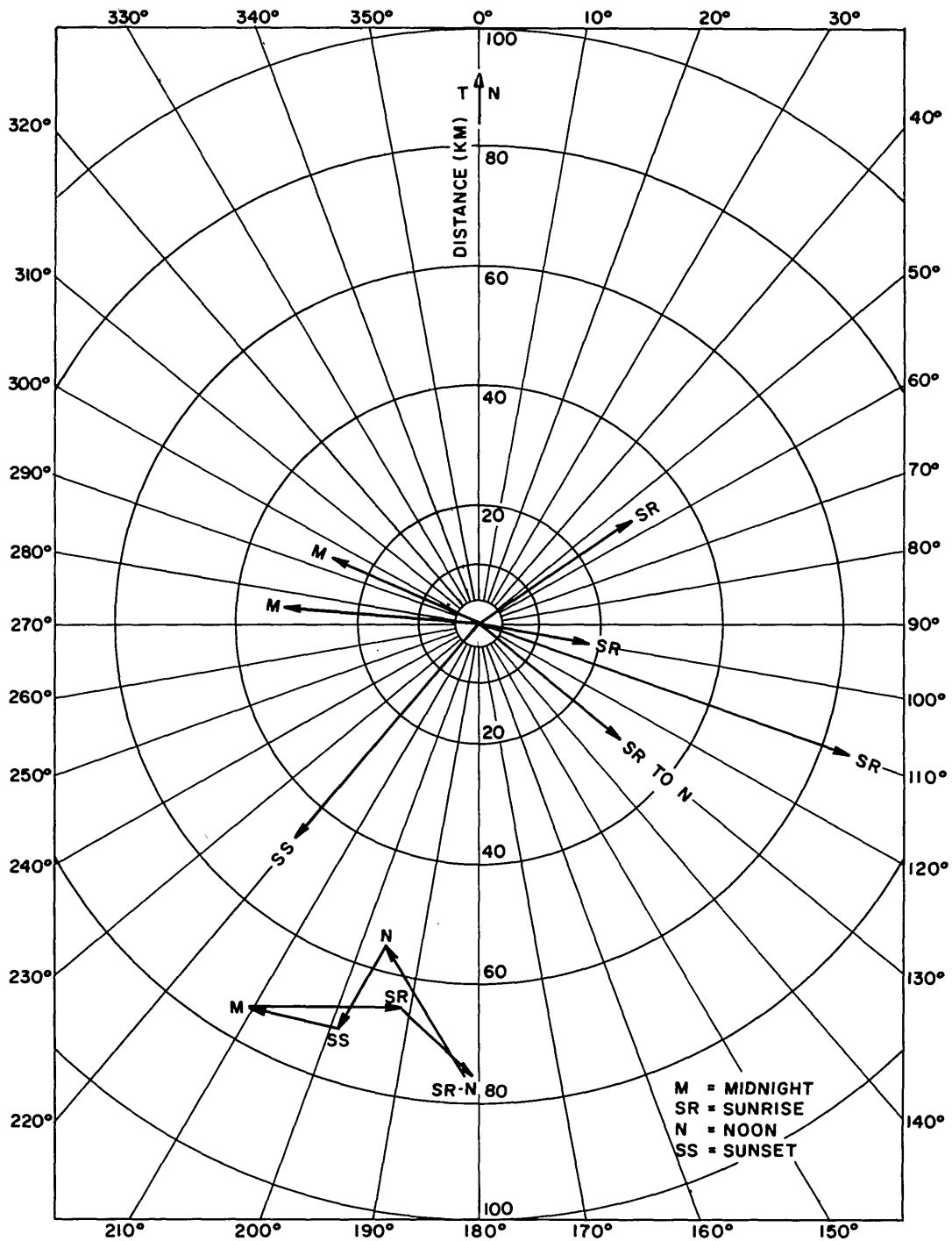


Fig. 11 — Polar plot of the movements of the electromagnetic antipode (EA) at different times of the local day as suggested by analysis of the NRL data

DOCUMENT CONTROL DATA - R&D

(Security classification of title, body of abstract and indexing annotation must be entered when the overall report is classified)

1. ORIGINATING ACTIVITY <i>(Corporate author)</i> U.S. Naval Research Laboratory Washington, D.C. 20390		2 a. REPORT SECURITY CLASSIFICATION Unclassified	
		2 b. GROUP	
3. REPORT TITLE RESULTS OF AIRBORNE FIELD MEASUREMENTS IN THE ANTIPODAL REGION OF RADIO STATION NPM, HAWAII			
4. DESCRIPTIVE NOTES <i>(Type of report and inclusive dates)</i> Final report on one phase of the problem.			
5. AUTHOR(S) <i>(Last name, first name, initial)</i> Rogerson, J. E.			
6. REPORT DATE April 26, 1966		7 a. TOTAL NO. OF PAGES 44	7 b. NO. OF REFS 10
8 a. CONTRACT OR GRANT NO. NRL Problem R01-39		9 a. ORIGINATOR'S REPORT NUMBER(S) NRL Report 6373	
b. PROJECT NO. SR 008-01-01, Task 7044		9 b. OTHER REPORT NO(S) <i>(Any other numbers that may be assigned this report)</i> None	
c.			
d.			
10. AVAILABILITY/LIMITATION NOTICES Distribution of this document is unlimited. Available from the Clearinghouse for Federal Scientific and Technical Information (CFSTI), Springfield, Va., 22151.			
11. SUPPLEMENTARY NOTES None		12. SPONSORING MILITARY ACTIVITY Department of the Navy (Bureau of Ships)	
13. ABSTRACT <p>The U.S. Naval Research Laboratory is conducting a comprehensive investigation of very-low-frequency (vlf) radio wave propagation. The objective of this investigation is to determine the parameters necessary for predicting the reliability of vlf communications in the ocean areas of the world.</p> <p>It is believed that an investigation of the electromagnetic fields at and near the antipode of a vlf transmitter would provide much propagation information. Since all the antipodes of the Navy vlf transmitter stations, except for station NPM in Hawaii, are located in remote ocean areas, this makes them operationally difficult to investigate, especially with respect to navigation. The NPM antipode, however, is located on land near Ghanzi, Bechuanaland Protectorate, in the Kalahari Desert in southern Africa. Navigation in the vicinity of the NPM antipode could conceivably be more precise than in other antipodal areas.</p> <p>An analysis of the data obtained in July 1963 by the Naval Research Laboratory via aircraft flights in the vicinity of the antipode of radio station NPM, Hawaii (19.8-kHz transmitter) is presented. Definite evidence of convergence of field strengths was found, as expected; a peak value of 2.0 mv/m for the field was measured during the experiment. Indications of an inverse square root dependence on distance for the field strength were observed. The expected diurnal pattern of highest field strengths at local sunrise, lowest fields at local sunset, and intermediate fields at local noon and midnight was found to be true. However, the antipodal situation appeared to be complex; suggestions of movement of the electromagnetic antipode were seen. Navigational difficulties contributed to uncertainties in the data and made definite conclusions difficult to obtain. The Navy Electronics Laboratory, San Diego, California, participated in this experiment by recording amplitude data at fixed ground sites around the geographic antipode and also phase data aboard the same aircraft. When the data taken by the two laboratories are combined, more comprehensive results may be obtainable.</p>			

Security Classification

14. KEY WORDS	LINK A		LINK B		LINK C	
	ROLE	WT	ROLE	WT	ROLE	WT
Radio signals Focusing Radio fields Ionosphere Atmospheric models Electromagnetic antipode Geographic antipode Very low frequency Propagation						

INSTRUCTIONS

1. ORIGINATING ACTIVITY: Enter the name and address of the contractor, subcontractor, grantee, Department of Defense activity or other organization (*corporate author*) issuing the report.

2a. REPORT SECURITY CLASSIFICATION: Enter the overall security classification of the report. Indicate whether "Restricted Data" is included. Marking is to be in accordance with appropriate security regulations.

2b. GROUP: Automatic downgrading is specified in DoD Directive 5200.10 and Armed Forces Industrial Manual. Enter the group number. Also, when applicable, show that optional markings have been used for Group 3 and Group 4 as authorized.

3. REPORT TITLE: Enter the complete report title in all capital letters. Titles in all cases should be unclassified. If a meaningful title cannot be selected without classification, show title classification in all capitals in parenthesis immediately following the title.

4. DESCRIPTIVE NOTES: If appropriate, enter the type of report, e.g., interim, progress, summary, annual, or final. Give the inclusive dates when a specific reporting period is covered.

5. AUTHOR(S): Enter the name(s) of author(s) as shown on or in the report. Enter last name, first name, middle initial. If military, show rank and branch of service. The name of the principal author is an absolute minimum requirement.

6. REPORT DATE: Enter the date of the report as day, month, year; or month, year. If more than one date appears on the report, use date of publication.

7a. TOTAL NUMBER OF PAGES: The total page count should follow normal pagination procedures, i.e., enter the number of pages containing information.

7b. NUMBER OF REFERENCES: Enter the total number of references cited in the report.

8a. CONTRACT OR GRANT NUMBER: If appropriate, enter the applicable number of the contract or grant under which the report was written.

8b, 8c, & 8d. PROJECT NUMBER: Enter the appropriate military department identification, such as project number, subproject number, system numbers, task number, etc.

9a. ORIGINATOR'S REPORT NUMBER(S): Enter the official report number by which the document will be identified and controlled by the originating activity. This number must be unique to this report.

9b. OTHER REPORT NUMBER(S): If the report has been assigned any other report numbers (*either by the originator or by the sponsor*), also enter this number(s).

10. AVAILABILITY/LIMITATION NOTICES: Enter any limitations on further dissemination of the report, other than those

imposed by security classification, using standard statements such as:

- (1) "Qualified requesters may obtain copies of this report from DDC."
- (2) "Foreign announcement and dissemination of this report by DDC is not authorized."
- (3) "U. S. Government agencies may obtain copies of this report directly from DDC. Other qualified DDC users shall request through _____."
- (4) "U. S. military agencies may obtain copies of this report directly from DDC. Other qualified users shall request through _____."
- (5) "All distribution of this report is controlled. Qualified DDC users shall request through _____."

If the report has been furnished to the Office of Technical Services, Department of Commerce, for sale to the public, indicate this fact and enter the price, if known.

11. SUPPLEMENTARY NOTES: Use for additional explanatory notes.

12. SPONSORING MILITARY ACTIVITY: Enter the name of the departmental project office or laboratory sponsoring (*paying for*) the research and development. Include address.

13. ABSTRACT: Enter an abstract giving a brief and factual summary of the document indicative of the report, even though it may also appear elsewhere in the body of the technical report. If additional space is required, a continuation sheet shall be attached.

It is highly desirable that the abstract of classified reports be unclassified. Each paragraph of the abstract shall end with an indication of the military security classification of the information in the paragraph, represented as (TS), (S), (C), or (U).

There is no limitation on the length of the abstract. However, the suggested length is from 150 to 225 words.

14. KEY WORDS: Key words are technically meaningful terms or short phrases that characterize a report and may be used as index entries for cataloging the report. Key words must be selected so that no security classification is required. Identifiers, such as equipment model designation, trade name, military project code name, geographic location, may be used as key words but will be followed by an indication of technical context. The assignment of links, roles, and weights is optional.